Molecular Pharmacology Fast Forward. Published on August 1, 2013 as doi:10.1124/mol.113.087247
This article has not been copyedited and formatted. The final version may differ from this version.

ROLE OF HUMAN HYPOXANTHINE GUANINE PHOSPHORIBOSYLTRANSFERASE IN ACTIVATION OF THE ANTIVIRAL AGENT T-705 (FAVIPIRAVIR)

Lieve Naesens, Luke Guddat, Dianne Keough, André B.P. van Kuilenburg, Judith Meijer, Johan Vande Voorde and Jan Balzarini

Rega Institute for Medical Research, KU Leuven, Minderbroedersstraat 10, B-3000, Leuven, Belgium: LN, JVV and JB

School of Chemistry and Molecular Biosciences, University of Queensland, Brisbane, 4072, QLD, Australia: LG and DK

Laboratory of Genetic Metabolic Diseases, Academic Medical Center, Amsterdam, The Netherlands: AVK and JM

Running Title: Phosphoribosylation of T-705 by human HGPRT

Corresponding author: Dr. Lieve Naesens, Rega Institute for Medical Research, KU Leuven, Minderbroedersstraat 10, B-3000 Leuven.

Tel. +32-1633745; fax +32-16337340; email: lieve.naesens@rega.kuleuven.be

Number of text pages: 35

Number of Tables: 5

Number of Figures: 6

Number of references: 52

Abstract: 243 words

Introduction: 750 words

Discussion: 1499 words

Abbreviations used: HGPRT, hypoxanthine guanine phosphoribosyltransferase; APRT, adenine phosphoribosyltransferase; NAMPT, nicotinamide phosphoribosyltransferase; RMP, ribose-5′-monophosphate metabolite; RTP, ribose-5′-triphosphate metabolite; ADK, adenosine kinase; PNP, purine nucleoside phosphorylase; *P*Rib-*PP*, 5-phospho-α-D-ribosyl-1-pyrophosphate.

Molecular Pharmacology Fast Forward. Published on August 1, 2013 as DOI: 10.1124/mol.113.087247
This article has not been copyedited and formatted. The final version may differ from this version.

ABSTRACT

6-Fluoro-3-hydroxy-2-pyrazinecarboxamide (T-705) is a novel antiviral compound with broad activity against influenza virus and diverse RNA viruses. Its active metabolite, T-705-ribose-5′-triphosphate (T-705-RTP), is recognized by influenza virus RNA polymerase as a substrate competing with GTP, giving inhibition of viral RNA synthesis and lethal virus mutagenesis. Which enzymes perform the activation of T-705 is unknown. We here demonstrate that human hypoxanthine guanine phosphoribosyltransferase (HGPRT) converts T-705 into its ribose-5′-monophosphate (RMP) prior to formation of T-705-RTP. The anti-influenza virus activity of T-705 and T-1105 (3-hydroxy-2-pyrazinamide; the analogue lacking the 6-fluoro atom) was lost in HGPRT-deficient MDCK cells. This HGPRT dependency was confirmed in human HEK293T cells undergoing HGPRT-specific gene knockdown followed by influenza virus ribonucleoprotein reconstitution. Knockdown for adenine phosphoribosyltransferase (APRT) or nicotinamide phosphoribosyltransferase did not change the antiviral activity of T-705 and T-1105. Enzymatic assays showed that T-705 and T-1105 are poor substrates for human HGPRT having K_m^{app} values of 6.4 and 4.1 mM, respectively. Formation of the RMP metabolites by APRT was negligible, and so was the formation of the ribosylated metabolites by human purine nucleoside phosphorylase. Phosphoribosylation and antiviral activity of the 2-pyrazinecarboxamide derivatives was shown to require the presence of the 3-hydroxyl but not the 6-fluoro substituent. The crystal structure of T-705-RMP in complex with human HGPRT showed how this compound binds in the active site. Since conversion of T-705 by HGPRT appears to be inefficient, T-705-RMP prodrugs may be designed to increase the antiviral potency of this new antiviral agent.

Molecular Pharmacology Fast Forward. Published on August 1, 2013 as DOI: 10.1124/mol.113.087247
This article has not been copyedited and formatted. The final version may differ from this version.

INTRODUCTION

Influenza viruses cause considerable medical and socio-economical burden, which is only partially addressed by current influenza vaccines (Osterhaus et al., 2011). Two classes of antiviral drugs are currently available: the M2 channel blockers amantadine and rimantadine, and the neuraminidase inhibitors (NAI) oseltamivir and zanamivir. Global spread of amantadine-resistant influenza viruses has largely excluded further use of this drug (Moscona, 2008). Moreover, virus resistance to oseltamivir is steadily rising (Moscona, 2009). Thus, new antiviral drugs with a different mode of action are needed to protect the population against seasonal influenza and sporadic pandemic outbreaks (Hayden, 2009). The novel antiviral compound T-705 [6-fluoro-3-hydroxy-2-pyrazinecarboxamide; Fig. 1], also called favipiravir, is recognized as particularly promising. This agent has broad *in vitro* activity against influenza A, B and C viruses (Furuta et al., 2002), including the highly pathogenic avian influenza H5N1 virus (Kiso et al., 2010), and virus strains with resistance to M2 blockers or NAI (Sleeman et al., 2010). T-705 produced strong protective effect when orally administered to mice infected with a lethal dose of H5N1 virus (Sidwell et al., 2007). The compound also appears to have a high barrier for selecting resistance, since no T-705-resistant influenza virus was obtained after thirty serial passages with T-705 in cell culture (Furuta et al., 2009). T-705 is currently undergoing Phase 2/3 trials for the treatment of uncomplicated influenza virus infections. Besides its activity against influenza virus, T-705 suppresses diverse RNA viruses such as arenaviruses (Gowen et al., 2007), bunyaviruses (Gowen et al., 2007), West Nile virus (Morrey et al., 2008) and norovirus (Rocha-Pereira et al., 2012), and T-705 therefore classifies as a broad anti-RNA virus agent (Furuta et al., 2009).

To exert its antiviral effect, T-705 acts as a nucleobase analogue which, after metabolic conversion into T-705-ribose-5′-triphosphate (T-705-RTP), functions as a competitive inhibitor of the influenza virus RNA polymerase (Furuta et al., 2005). Cell culture metabolism

Molecular Pharmacology Fast Forward. Published on August 1, 2013 as DOI: 10.1124/mol.113.087247
This article has not been copyedited and formatted. The final version may differ from this version.

studies with radiolabeled T-705 indicated that it is first converted into its ribose-5′-monophosphate (T-705-RMP) metabolite, followed by phosphorylation to T-705-RTP (Furuta et al., 2005). The latter is the assumed antivirally active form since it was shown, in an enzymatic assay, to be a GTP-competitive inhibitor of the influenza virus RNA polymerase having a 50% inhibitory concentration of 0.14 μM (Furuta et al., 2005). Since T-705-RTP has a natural ribose moiety, its incorporation into viral RNA may possibly allow further RNA chain elongation and drive the virus into lethal mutagenesis. Alike the broad antiviral nucleoside analogue ribavirin, T-705 possesses a rotating carboxamide function which makes it both a potential guanine and adenine mimicking 'pseudobase' (Fig. 2). Thus, the lethal virus mutagenesis concept first described for ribavirin (Crotty et al., 2000) may also apply to T-705. It was recently demonstrated that serial cell culture passage of influenza virus in the presence of T-705 gives rise to a non-viable virus phenotype with marked enrichment in G-to-A and C-to-T mutations (Baranovich et al., 2013).

The enzymes that are responsible for activation of T-705 remain to be established. A quantitative analysis of the intracellular conversion of T-705 into T-705-RTP was performed by Smee et al. (2009), who showed that the formation of T-705-RTP in Madin-Darby canine kidney (MDCK) cells is dose-proportional and reaches a plateau after about 9 h incubation with compound. The efficiency of T-705-RTP formation was similar in uninfected *versus* influenza virus-infected MDCK cells. These authors proposed that hypoxanthine guanine phosphoribosyltransferase (HGPRT) could perform the first step in the activation pathway of T-705, but no experimental data were provided to substantiate this hypothesis. In the study presented here, we demonstrate for the first time that T-705 absolutely depends on the cellular HGPRT enzyme to exert its anti-influenza virus activity in mammalian cells. Two other phosphoribosyltransferases, adenine phosphoribosyltransferase (APRT) and nicotinamide phosphoribosyltransferase (NAMPT) were shown to play no relevant role in the cellular

Molecular Pharmacology Fast Forward. Published on August 1, 2013 as DOI: 10.1124/mol.113.087247
This article has not been copyedited and formatted. The final version may differ from this version.

activation of T-705. Two distantly related carboxamide compounds (Fig. 1) were examined in parallel: ribavirin, which is activated by ADK (Willis et al., 1978) [although other enzymes such as cytosolic 5′-nucleotidase II (Wu et al., 2005) may also be involved]; and the base of ribavirin, which was reported to be a substrate for purine nucleoside phosphorylase (PNP) (Streeter et al., 1977). We determined the structural requirements for recognition of T-705 and related 2-pyrazinecarboxamide compounds by human HGPRT, and the catalytic efficiency for conversion of T-705 and its non-fluorinated analogue T-1105 into their phosphoribosylated metabolites. The crystal structure of human HGPRT in complex with T-705-RMP was obtained and revealed how this compound interacts with active site amino acid residues.

Molecular Pharmacology Fast Forward. Published on August 1, 2013 as DOI: 10.1124/mol.113.087247
This article has not been copyedited and formatted. The final version may differ from this version.

MATERIALS AND METHODS

Chemical compounds

The chemical structures of T-705 and its structural analogues are shown in Fig. 1. The sources of these compounds were: T-705 (6-fluoro-3-hydroxy-2-pyrazinecarboxamide), from YouChemicals (Shanghai, China); T-1105 (3-hydroxy-2-pyrazinecarboxamide), from Santa Cruz Biotechnology; 2-pyrazinecarboxamide and 6-chloro-3,5-diamino-2-pyrazinecarboxamide, both from Sigma-Aldrich. Ribavirin (Virazole®) was from ICN Pharmaceuticals, whereas its free base (1,2,4-triazole-3-carboxamide) was purchased from TCI Europe (Zwijndrecht, Belgium). 6-Thioguanine (TG) and all other cytostatic agents were from Sigma-Aldrich. Stock solutions of these chemical agents were prepared in 100% DMSO at a concentration of 10 to 50 mM. For experiments requiring high concentrations of T-705 or T-1105 (i.e. K_m^{app} determinations), a 500 mM stock solution was used. DMSO concentrations were ≤0.1% in the cellular assays, and ≤1% in the enzymatic tests; it was ascertained that these DMSO concentrations had no effect on the outcome of the cellular or enzymatic experiments.

Anti-influenza virus and cytotoxicity assays

The detailed procedures to determine the anti-influenza virus activity in Madin-Darby canine kidney (MDCK) cells can be found elsewhere (Vanderlinden et al., 2010). The cell culture medium consisted of Dulbecco's Modified Eagle Medium (Invitrogen), supplemented with 10% fetal calf serum, 1 mM sodium pyruvate and 0.075% sodium bicarbonate. The medium used during virus infections consisted of Ultra MDCK® medium (Lonza), supplemented with 0.0225% sodium bicarbonate, 2 mM L-glutamine and 2 µg/mL TPCK (tosylphenylalanylchloromethylketon)-treated trypsin (from Sigma-Aldrich). The influenza virus strains used were: A/PR/8/34 (A/H1N1); A/X-31 and A/HK/7/87 (A/H3N2); and

Molecular Pharmacology Fast Forward. Published on August 1, 2013 as DOI: 10.1124/mol.113.087247
This article has not been copyedited and formatted. The final version may differ from this version.

B/HK/5/72 (Vanderlinden et al., 2012). MDCK cells, seeded in 96-well plates, were infected with virus at a multiplicity of infection of 0.0004 plaque forming units per cell. At the same time, serial dilutions of the test compounds were added. After three days incubation at 35°C, microscopy was performed to estimate the inhibitory effect of the compounds on virus-induced cytopathic effect (CPE), as well as their cytotoxic activity. These microscopic data were confirmed by the spectrophotometric formazan-based MTS cell viability assay. Antiviral activity was expressed as the EC_{50} value, or compound concentration producing 50% protection against virus-induced CPE. The MCC represented the concentration causing microscopically visible changes in cell morphology, and the CC_{50} was the concentration causing 50% reduction in cell viability.

For virus yield experiments, virus infection and compound treatment were performed as above. At 24 h after infection, the cell culture supernatants were collected and frozen at -80°C. Virus lysis and one-step real-time RT-PCR quantification of viral RNA copies were performed as described, using an M-gene directed primer set and probe (Stevaert et al., 2013). The antiviral activity was expressed as the EC_{90} or EC_{99}, or compound concentrations producing a 1-$\log_{10}$ or 2-$\log_{10}$ reduction in virus titer, respectively.

To determine the cytostatic activity of diverse nucleoside analogues in wild-type or HGPRT-deficient MDCK cell cultures (see below), the cells were seeded into 96-well plates at 15000 cells per well and incubated with serial compound dilutions. After three days incubation at 37°C, the cells were trypsinized and counted with a Coulter Counter (Analis, Suarlée, Belgium). The IC_{50}, or compound concentration affording 50% inhibition of cell proliferation, was calculated by interpolation.

Molecular Pharmacology Fast Forward. Published on August 1, 2013 as DOI: 10.1124/mol.113.087247
This article has not been copyedited and formatted. The final version may differ from this version.

Selection and characterization of HGPRT-deficient MDCK cells

MDCK cells were seeded in 6-well plates and treated with 6-thioguanine at a final concentration of 25 to 100 µM. After ten days incubation at 37°C, floating dead cells were removed, and surviving cells were detached with trypsin-EDTA and subcultivated in 100 or 200 µM 6-thioguanine. After another ten days, the surviving cells were transferred to a 96-well plate and incubated with 100 or 200 µM 6-thioguanine in conditioned culture medium. After allowing cell proliferation for a total of six weeks, the cells were seeded in 96-well plates at an estimated density of 1 cell per well. Eleven individual TG-resistant cell clones were selected, expanded and characterized (see below). One selected clone (designated MDCK-TG^{res}) was kept in culture with continuous addition of 200 µM 6-thioguanine. No signs of reversal of the TG-resistant phenotype were seen during the course of the study (~50 serial passages). Prior to their use in experiments, the cells were grown for one passage in the absence of 6-thioguanine.

HGPRT protein expression in the TG-resistant cell clones was assessed by Western blot analysis under denaturating and reducing conditions. Total cell lysates were prepared with the protein extraction buffer described (De Bolle et al., 2002). Twelve µg of total protein was loaded on 12% Tris-glycine gels. After electrophoresis and transfer to PVDF membranes, the blots were stained with anti-HGPRT antibody (rabbit polyclonal; Abcam ab10479; final dilution 1/1000), or anti-β-actin antibody (Sigma-Aldrich A5441; dilution 1/5000), followed by a horseradish peroxidase-linked secondary antibody (anti-rabbit: Dako P0399; dilution 1/4000, or anti-mouse: Dako P0477; dilution 1/1000). The antibodies were diluted in 2% nonfat dry milk in PBS-T (PBS with 0.1% Tween). Visualization of the protein bands was done with the ECLplus reagent from GE Healthcare, followed by exposure to X-ray film.

To assess the HGPRT enzymatic activity in the TG-resistant MDCK cell clones, monolayer cultures of wild-type and MDCK-TG^{res} cells were exposed to [2,8-^{3}H]Hx (specific

Molecular Pharmacology Fast Forward. Published on August 1, 2013 as DOI: 10.1124/mol.113.087247
This article has not been copyedited and formatted. The final version may differ from this version.

radioactivity: 15 Ci/mmol) at 2 µCi per 5 mL culture medium (final concentration: 0.027 µM). After 24 h incubation at 37°C, the cultures were washed three times with serum-free culture medium at room temperature, and then trypsinized. The cells were centrifuged, washed once with culture medium, and the cell pellet was extracted with ice-cold methanol (66%). After standing on ice for 15 min, the methanol-insoluble fraction was collected by centrifugation (13,400 *g*; 10 min; 4°C) and then counted for radioactivity. The supernatants were subjected to HPLC analysis to separate [2,8-^{3}H]Hx-derived metabolites and collected eluate fractions were submitted to scintillation counting.

To determine the genetic basis for the HGPRT deficiency of the selected MDCK-TG^{res} cell clone, sequence analysis of HGPRT-encoding cDNA and gDNA was performed. DNA was isolated from wild-type and MDCK-TG^{res} cells using standard techniques. PCR amplification of all nine coding exons and flanking intronic regions of *HPRT (dog)* was carried out using intronic primer sets (primer sequences available upon request). Amplification of gDNA of *HPRT (dog)* exon 1-2 was carried out in 25-µL reaction mixtures containing 25 mM TAPS.HCl pH 9.3; 50 mM KCl, 2 mM $MgCl_2$, 1 mM ß-mercaptoethanol, 0.5 µM of each primer, 0.2 mM dNTPs and 0.02 U of Q5 Hot Start High-Fidelity polymerase (New England Biolabs). After initial denaturation for 5 min at 98°C, amplification was carried out for 35 cycles (10 s 98°C, 30 s 65°C, 15 s 72°C) with a final extension step of 2 min at 72°C. Amplification of gDNA of *HPRT (dog)* exon 3-9 was carried out in 25-µL reaction mixtures containing 20 mM Tris-HCl pH 8.4, 50 mM KCl, 1.5 mM $MgCl_2$, 0.4 µM of each primer, 0.2 mM dNTPs and 0.025 U of Platinum Taq polymerase (Invitrogen). After initial denaturation for 5 min at 95°C, amplification was carried out for 30 cycles (30 s 95°C, 30 s 55°C, 1 min 72°C) with a final extension step of 10 min at 72°C. In parallel, total RNA was isolated from wild-type and MDCK-TG^{res} cells using Trizol extraction (Invitrogen). cDNA was prepared by RT-PCR using a transcriptor first strand cDNA synthesis kit (Roche). PCR amplification of

Molecular Pharmacology Fast Forward. Published on August 1, 2013 as DOI: 10.1124/mol.113.087247
This article has not been copyedited and formatted. The final version may differ from this version.

cDNA of *HPRT (dog)* was performed using primer sets spanning exons 1-3, exons 4-8, or exon 9 (sequences available upon request). Amplification of cDNA was carried with Platinum Taq polymerase in 25-µL reaction mixtures and using the PCR protocol as described above. PCR products were separated on a 1.5% agarose gel and visualized with ethidium bromide, or used for direct sequencing.

vRNP reconstitution assay after gene knockdown

Gene knockdown was performed with ON-TARGETplus SMARTpool siRNAs from Dharmacon, directed towards the human genes HPRT1, ADK, APRT or NAMPT, or with a non-targeting negative control. The siRNAs were reconstituted and frozen in aliquots as recommended by the manufacturer. The pHW2000-based bidirectional plasmids for reconstitution of the vRNP segments (i.e. encoding PA, PB1, PB2 and NP) from influenza A/WSN/33 were a kind gift from Dr. R. Webster (St. Jude Children's Research Hospital, Memphis, USA) (Hoffmann et al., 2000). The firefly luciferase reporter plasmid, which contains the firefly luciferase coding sequence flanked by the 5′- and 3′-UTR sequences from the A/Puerto Rico/8/34 NS gene, was kindly provided by Dr. M. Kim (Korea Research Institute of Chemical Technology, Daejeon), while the Renilla luciferase reporter plasmid was the pRL-TK plasmid (containing an HSV TK promoter) from Promega.

To transfect the siRNAs into human embryonic kidney HEK293T cells, the cells were seeded in 2 mL culture medium, at 700,000 cells per well in 6-well plates. One day later, the siRNAs were mixed with Lipofectamin RNAiMAX, which was first diluted in Opti-MEM I (both from Invitrogen). After 20 min incubation at room temperature, 500 µL transfection mixture was slowly added to the cells at a final siRNA concentration of 40 nM and a volume of 5 µL Lipofectamin RNAiMAX per well. An extra condition of untransfected control cells was included. After 48 h incubation at 37°C, the cells were trypsinized, resuspended in culture

Molecular Pharmacology Fast Forward. Published on August 1, 2013 as DOI: 10.1124/mol.113.087247
This article has not been copyedited and formatted. The final version may differ from this version.

medium at 15 x 10^6 cells per mL, and transfected with the four vRNP reconstituting plasmids and the firefly and Renilla luciferase reporter plasmids. The procedure (Meneghesso et al., 2013) was adapted from the reverse genetics protocol published by Martínez-Sobrido and Garcia-Sastre (2010). Specifically, 1 mL of the transfection mixture contained: 2.4 x 10^6 siRNA-treated HEK293T cells; 5 µL Lipofectamin-2000 (from Invitrogen); 0.22 µg of each of the four vRNP-reconstituting plasmids; 0.086 µg of the firefly luciferase plasmid, and 0.020 µg of the Renilla luciferase plasmid. This mixture was transferred to a 96-well plate (50 µL per well) containing 10 µL of the antiviral compounds at serial dilutions, and the plate was incubated during 24 h at 37°C. Luciferase activity was determined using the Dual-Glo® assay system from Promega.

To determine the gene knockdown efficiency, protein extracts were prepared at 48 h after siRNA transfection. The extraction buffer and SDS-PAGE conditions were the same as mentioned above. The blots were stained with the primary antibodies: anti-HGPRT and anti-β-actin: same as above; anti-APRT (mouse polyclonal; Abcam ab72782; 1/1000); anti-NAMPT (rabbit polyclonal; Abcam ab24149; 1/1000); and anti-ADK (a rabbit polyclonal that was generously donated by D. Boison, Portland, Oregon, USA; 1/5000) (Masino et al., 2011). Exposure to the secondary antibodies and detection of the protein bands was done as described above. The band intensity was quantified with ImageQuant TL 7.0 software from GE Healthcare.

In addition, gene knockdown efficiency for HGPRT and APRT was estimated by determining the cytostatic activity of 6-thioguanine and 2,6-diaminopurine in HEK293T cells following siRNA transfection. First, the HEK293T cells were seeded in 6-well plates and transfected with siRNA for HGPRT, APRT or non-targeting negative control, as described above. At 24 h after transfection, the cells were trypsinized, resuspended in culture medium at 0.8 x 10^6 cells per mL, and transferred to a 96-well plate (100 µL per well) containing 20 µL of 6-

Molecular Pharmacology Fast Forward. Published on August 1, 2013 as DOI: 10.1124/mol.113.087247
This article has not been copyedited and formatted. The final version may differ from this version.

thioguanine or 2,6-diaminopurine at serial dilutions. After 48 h incubation at 37°C, the cells were counted with a Coulter Counter and the IC_{50} values were calculated as described above.

Enzymatic assays with HGPRT, APRT and PNP

The following recombinant enzymes, produced in *E. coli*, were purchased from Prospec Bio (Rehovot, Israel): N-terminal His-tagged human HGPRT (EC 2.4.2.8); human APRT (EC 2.4.2.7); and N-terminal His-tagged purine nucleoside phosphorylase (PNP; EC 2.4.2.1). In the case of HGPRT, the reaction mixture contained 100 mM Tris-HCl at pH 7.4, 10 mM $MgCl_2$, and, depending on the base substrate, 0.2 or 7 mM 5-phospho-α-D-ribosyl-1-pyrophosphate (*P*Rib-*PP*) and 0.019 or 0.37 µM of the enzyme. For APRT, the reaction conditions were 50 mM Tris-HCl at pH 7.4, 5 mM $MgCl_2$, 1 µg per µL BSA and, depending on the base substrate, 0.05 or 7 mM *P*Rib-*PP* and 0.051 or 0.77 µM of the enzyme. The samples (50 µL total volume) were incubated at 37°C during the indicated times. After stopping the reaction with 100 µL ice-cold methanol and sample clarification by centrifugation (13,400 *g*; 10 min; 4°C), the samples were analyzed by anion-exchange HPLC using a Partisphere SAX column (4.6 x 125 mm) from Whatman. Elution was performed with buffer A and buffer B, containing 5 mM and 0.3 M ammonium dihydrogen phosphate, respectively (both at pH 5.0), a flow rate of 1.5 ml per min, and the following gradient system: 0-5 min: 100% A; 5-13 min: to 90% A and 10% B; 13-15 min: 90% A and 10% B; 15-20 min: to 100% A; 20-30 min: 100% A. UV absorbance was measured with a Waters 996 photodiode array detector. The retention times and λ_{max} values of the enzyme reaction products were: for T-705-RMP: 12.1 min and 372 nm; for T-1105-RMP: 12.1 min and 348 nm; for GMP: 20.2 min and 252 nm; for IMP: 16.0 min and 247 nm; and for AMP: 16.3 min and 258 nm. The formation of GMP or IMP (by HGPRT), or AMP (by APRT) was calculated by constructing standard curves from external standards of GMP, IMP or AMP. Since

Molecular Pharmacology Fast Forward. Published on August 1, 2013 as DOI: 10.1124/mol.113.087247
This article has not been copyedited and formatted. The final version may differ from this version.

standards of T-705-RMP and T-1105-RMP were not available, the amounts of T-705 and T-1105 converted were determined by quantifying the amount of parent compound remaining after the enzyme reaction. To this purpose, the extracts were also separated on a Superspher 100 RP-18 reverse-phase column (4 µm; 4 x 250 mm) from Merck. Elution was performed (at 1 ml per min) with acetonitrile (D) and buffer C: 50 mM ammonium dihydrogen phosphate and 5 mM 1-heptane sulfonic acid, pH 3.2. The gradient system was: 0-5 min: 100% C; 5-35 min: to 60% C and 40% D; 35-40 min: 60% C and 40% D; 40-50 min: to 100% C; 50-60 min: 100% C. The RT of T-705 was 22.0 min and its λ_{max} was 321 nm; for T-1105, the corresponding parameters were: 4.7 min and 348 nm.

To determine the apparent K_m (K_m^{app}) and k_{cat} values for phosphoribosylation of T-705 and T-1105 by HGPRT, the compounds were incubated with 7 mM *P*Rib-*PP* and 0.37 µM enzyme for 6 h, at substrate concentrations ranging from 0.156 to 5 mM (the highest concentration attainable). The K_m^{app} and k_{cat} values of hypoxanthine and guanine were determined under conditions of 0.2 mM *P*Rib-*PP* and 0.019 µM HGPRT, different concentrations of hypoxanthine or guanine (in the range of 0.9-77 µM), and an incubation time of 5 min. Similar experiments were done with the APRT enzyme. T-705 or T-1105 (at 0.156 to 5 mM concentrations) were incubated for 6 h with 7 mM *P*Rib-*PP* and 0.77 µM APRT enzyme. The K_m^{app} value for adenine was determined under conditions of 0.9-77 µM adenine, 0.05 mM *P*Rib-*PP* and 0.051 µM enzyme, and an incubation time of 2.5 min. Kinetic parameters (K_m^{app} and k_{cat}) were calculated by non-linear regression analysis, using GraphPad (6.02) software.

To identify the T-705-RMP metabolite, T-705 was first incubated with 0.37 µM of the HGPRT enzyme during 24 h. Then, calf intestine alkaline phosphatase (from Roche; final concentration: 10 units per 100 µL) and dephosphorylation buffer (pH 8.5; also from Roche) were added and the samples were again incubated during 60 min. After addition of methanol

Molecular Pharmacology Fast Forward. Published on August 1, 2013 as DOI: 10.1124/mol.113.087247
This article has not been copyedited and formatted. The final version may differ from this version.

and sample clarification, the extracts were subjected to RP18-HPLC analysis as described above.

The PNP assay conditions to estimate ribosylation of T-705 or T-1105 (at a concentration of 5 mM) were: 50 mM HEPES pH 7.5, 7 mM ribose-1-phosphate and 0.058 µM human PNP. After 6 or 24 h incubation at 37 °C, the reaction was stopped by heat inactivation of the enzyme (3 min at 95°C). The samples were clarified (13,400 *g*; 10 min; 4°C), and then analyzed by RP18-HPLC as described above. A similar experiment was performed to follow conversion of hypoxanthine to inosine after 5 to 60 min incubation, in a reaction mixture containing 100 µM hypoxanthine, 1 mM ribose-1-phosphate and 0.0029 µM PNP enzyme.

Crystallization and structure determination of human HGPRT in complex with T-705-RMP

To perform crystallization experiments, purified recombinant hexa-histidine tagged human HGPRT was concentrated to 0.67 mM, in terms of subunits. The enzyme was stored at -70°C in 0.1 M Tris-HCl pH 7.4, 0.01 M $MgCl_2$, 1 mM DTT and 300 mM *P*Rib-*PP*. Prior to crystallization, the enzyme ($[E]_o$, in terms of subunits, 0.67 mM) was pre-incubated with T-705 (at 7.2 mM), *P*Rib-*PP* (at 3 mM) and a final DMSO concentration of 5%, for 10 min at 5°C. Crystals were obtained by the hanging drop method, where 1 µL of reservoir solution and 1 µL of the complex were combined and incubated at 18°C. The reservoir solution was composed of 0.2 M NaCl, 1 M sodium/potassium tartrate, 0.1 M imidazole, pH 8.0. Crystals appeared within two weeks. For crystallization in the absence of T-705, human HGPRT was incubated with 3 mM *P*Rib-*PP* and 5% DMSO.

After cryocooling the crystals at 100 K, the X-ray data were collected using Beamline MX1 of the Australian Synchrotron. The data sets were scaled and merged using Xds (Kabsch, 2010). The structure was solved by molecular replacement using the program PHASER

(McCoy et al., 2007) within PHENIX 1.7.3 and the protein coordinates of human HGPRT in complex with GMP (PDB code 1HMP). Subsequent refinement of the coordinates was with PHENIX (Adams et al., 2010) and model building with COOT (Emsley et al., 2010). The structural restraints for the ligand were generated using the PRODRG2 Dundee server (Schuttelkopf and van Aalten, 2004). The coordinates and structure factors were submitted to the Protein Data Bank (accession number: 4KN6).

Molecular Pharmacology Fast Forward. Published on August 1, 2013 as DOI: 10.1124/mol.113.087247
This article has not been copyedited and formatted. The final version may differ from this version.

RESULTS

Anti-influenza virus activity of T-705 and related structural analogues

We first verified whether T-705 has selective antiviral activity in our stringent CPE reduction assay in MDCK cells, using three influenza virus strains belonging to the A/H1N1, A/H3N2 or B (sub)type. Three commercially available structural analogues of T-705 (see Fig. 1 for chemical structures) were tested in parallel. As shown in Table 1, the antiviral EC_{50} values of T-705 were similar for the three influenza viruses, and comparable values were obtained by the CPE and MTS assay, yielding an average EC_{50} value of 10 µM for T-705. This value is ~10-fold higher compared with the EC_{50} value reported by Furuta et al. (2002), but in the same range as recently reported by Baranovich et al. (2013). No signs of cytotoxicity were observed at 500 µM T-705 (the highest concentration tested), yielding a selectivity index (ratio of cytotoxic to antiviral concentration) of at least 50. The reference compound ribavirin, a nucleoside analogue which alike T-705 possesses a carboxamide function and broad anti-RNA virus activity, displayed comparable EC_{50} values as T-705 but considerably higher cytotoxicity. Interestingly, T-1105 was ~4-fold more potent than T-705 and also not cytotoxic at 500 µM, meaning that the 6-fluoro atom of T-705 is not required to obtain selective anti-influenza virus activity. On the other hand, no antiviral activity was noted for 2-pyrazinamide (which lacks the 3-hydroxyl group) and the 6-chloro-3,5-diamino-2-pyrazinamide analogue. Also, the free ribavirin base (i.e. lacking the ribose moiety; Fig. 1) did not display anti-influenza virus activity. The antiviral EC_{50} values of nucleozin, a non-nucleoside analogue which acts by aggregating the influenza virus nucleoprotein, were in the same range as the values reported in the literature (Kao et al., 2010); this compound proved to be inactive against influenza B virus.

Molecular Pharmacology Fast Forward. Published on August 1, 2013 as DOI: 10.1124/mol.113.087247
This article has not been copyedited and formatted. The final version may differ from this version.

Anti-influenza virus activity of T-705 in wild-type *versus* HGPRT-deficient cells

Cells lacking a functional HGPRT enzyme were considered well suited to assess the role of HGPRT in the potential metabolic activation and antiviral activity of T-705 (Fig. 2). We initially performed experiments with HGPRT-deficient human melanoma C32-TG cells (Chen, 1983). In these cells, T-705 was not active against respiratory syncytial virus, vesicular stomatitis virus and Punta Toro virus, while being moderately active (EC_{50} values in the range of 40 μM) in wild-type C32 cells (data not shown). Since the C32-TG cells did not support influenza virus replication, we decided to select an HGPRT-deficient MDCK cell clone using the HGPRT-dependent cytotoxic agent 6-thioguanine (Chen, 1983). After eight serial passages of MDCK cells in the presence of 100 to 200 μM 6-thioguanine, followed by subcloning of the surviving cells, one 6-thioguanine-resistant MDCK cell clone was designated MDCK-TG^{res} and selected for further experiments. First, a detailed phenotypic and genotypic analysis was undertaken. The absence of HGPRT protein in the MDCK-TG^{res} cells was demonstrated by Western blot analysis, using an antibody directed to the C-terminal part of HGPRT (Fig. 3A). Wild-type MDCK (MDCK-WT) cells showed efficient incorporation of [2,8-^{3}H]Hx into their purine nucleotide pools (Fig. 3C; left panel), resulting in marked incorporation of radioactivity into cellular nucleic acids contained in the methanol-insoluble fraction (Fig. 3C; right panel). In contrast, the MDCK-TG^{res} cells were heavily compromised in using hypoxanthine as a metabolic precursor for their purine nucleotide synthesis.

The MDCK-TG^{res} cells were further characterized by comparing their HPRT gDNA and cDNA sequences to those of MDCK-WT cells. Analysis of the genomic sequences of exons 1-9 of *HPRT1 (dog)* and flanking intronic sequences showed that the MDCK-TG^{res} cells were heterozygous for a c.119G>A (p.G40E) mutation in exon 2. The glycine at position 40 proved to be highly conserved in *HPRT1* from mammals and other eukaryotes and the G40E

Molecular Pharmacology Fast Forward. Published on August 1, 2013 as DOI: 10.1124/mol.113.087247
This article has not been copyedited and formatted. The final version may differ from this version.

mutation can be predicted to be deleterious, consistent with the clinical observation that substitution of this Gly-40 or its surrounding residues leads to severe HGPRT deficiency (Jinnah et al., 2000). In parallel, RNA isolated from MDCK-WT and MDCK-TG^{res} cells was subjected to RT-PCR analysis. In MDCK-WT cells, a normal sized fragment of 461 bp corresponding to exons 1-3 was detected, whereas the MDCK-TG^{res} cells contained the 461 bp fragment together with a smaller sized fragment of 354 bp (Fig. 3B). Sequence analysis of the PCR fragments showed that the 354 bp fragment originated from the 461 bp fragment by a deletion of 107 bp, corresponding to the nucleotides c.28_134 of exon 2. This exon 2 deletion leads to a shifted reading frame resulting in a premature stop codon shortly afterwards (p.Ile10AspfsX2).

Finally, to further characterize the mutant MDCK cells, the MDCK-TG^{res} and MDCK-WT cells were compared for their sensitivity to a variety of cytostatic nucleoside analogues. The IC_{50} values (compound concentrations affording 50% inhibition of cell proliferation) obtained in the two cell lines are given in Table 2. As expected, the MDCK-TG^{res} cells were strongly resistant ($IC_{50} \geq 440$ µM) to the cytostatic effect of HGPRT-dependent nucleoside analogues, i.e. 6-thioguanine, 6-mercaptopurine and 6-thioguanosine. Presumably, the latter compound is preferentially hydrolyzed to 6-thioguanine by PNP prior to its HGPRT-directed conversion to 6-thioguanosine-5′-monophosphate. For the other nucleoside analogues, which use different mechanisms for their metabolic activation or cytotoxic action (see Legend to Table 2), the IC_{50} values were virtually identical in the WT and HGPRT-deficient MDCK cells. Thus, the 6-thioguanine resistant phenotype of the MDCK-TG^{res} cells was proven to be solely based on the lack of a functional HGPRT enzyme.

To investigate whether the HGPRT deficiency of the MDCK-TG^{res} cells renders them less sensitive to the antiviral action of T-705 and T-1105, a PCR-based virus yield assay was performed (Stevaert et al., 2013). The compounds were added to MDCK-TG^{res} or MDCK-WT

Molecular Pharmacology Fast Forward. Published on August 1, 2013 as DOI: 10.1124/mol.113.087247
This article has not been copyedited and formatted. The final version may differ from this version.

cells together with influenza virus and, after 24 h incubation, the virions released in the supernatant were quantified by RT-qPCR. Viral copy numbers in the untreated virus controls were similar for MDCK-TG^{res} and MDCK-WT cells (data not shown), meaning that the virus replicated with comparable efficiency in both cell lines. In MDCK-WT cells, the EC_{99} values of T-705, T-1105 and ribavirin obtained by the virus yield assay were 12, 2.5 and 3.6 µM, respectively (Table 3); these data are similar to the corresponding EC_{50} values obtained in the CPE reduction assay (see above). Of these three compounds, only ribavirin retained its antiviral activity in MDCK-TG^{res} cells. Its EC_{90} and EC_{99} values were about 3-fold lower in MDCK-TG^{res} compared to MDCK-WT cells, which might be explained by the fact that the MDCK-TG^{res} cells are unable to salvage IMP from hypoxanthine, increasing their sensitivity to the inhibitory effect of ribavirin 5′-monophosphate on IMP dehydrogenase. The finding that T-705 and T-1105 are totally devoid of antiviral activity in the HGPRT-deficient cells indicates that these two compounds are strictly dependent on activation by HGPRT. The other three carboxamide analogues, i.e. 2-pyrazinamide, 6-chloro-3,5-diamino-2-pyrazinamide and the RBV base, had no anti-influenza virus activity in the virus yield assay, confirming the results obtained in the CPE assay.

Effect of siRNA-mediated HGPRT knockdown on the inhibitory activity of T-705 towards influenza virus polymerase

The influenza virus ribonucleoprotein (vRNP) reconstitution assay represents a convenient cell-based method to estimate the activity of compounds towards the influenza virus polymerase (Meneghesso et al., 2013). In this plasmid-based assay, the four influenza virus proteins constituting the vRNP complexes are generated in human HEK293T cells. The transfection mixture also contains two reporter plasmids, i.e. a firefly luciferase encoding plasmid for which transcription depends on the activity of the viral vRNP, and a Renilla

Molecular Pharmacology Fast Forward. Published on August 1, 2013 as DOI: 10.1124/mol.113.087247
This article has not been copyedited and formatted. The final version may differ from this version.

luciferase control plasmid, for which transcription is solely dependent on cellular RNA polymerase II. Upon addition of a test compound, the firefly luciferase and Renilla luciferase signals are indicators for its inhibitory effect on the viral vRNP and cellular RNA polymerase II, respectively, thus corresponding to its antiviral activity and cytotoxicity, respectively. T-705 and T-1105 were shown to suppress influenza virus vRNP activity in a concentration-dependent manner, with 50% effective concentration (EC_{50}) values of 11 and 38 μM, respectively [see non-siRNA-transfected control cells (CC) in Table 4], and no inhibition of cellular RNA polymerase II at 500 μM (the highest concentration tested). Ribavirin was two times more potent than T-705 (EC_{50} of 5.2 μM) with no apparent toxicity at 500 μM. The NP aggregating agent nucleozin (for which vRNP inhibition is unrelated to an effect on the viral polymerase) (Kao et al., 2010) had an EC_{50} of 1.8 μM and an IC_{50} (concentration causing 50% reduction of the Renilla luciferase signal) of 43 μM.

The vRNP assay was used in gene knockdown experiments to verify that, among the three phosphoribosyltransferases that could be considered (i.e. HGPRT, APRT or NAMPT), HGPRT is the sole enzyme involved in intracellular activation of T-705. HEK293T cells were subjected to siRNA-mediated gene silencing for HGPRT, APRT or NAMPT; as controls, we included siRNA for ADK, reported to perform the first phosphorylation of ribavirin (Willis et al., 1978), or a negative control siRNA provided by the manufacturer. At 48 h after siRNA transfection, the cells were trypsinized to reconstitute the influenza vRNP and the compounds were added. After an additional 24 h, the dual luciferase assay was performed. In parallel, gene knockdown efficiency was measured at 48 h after siRNA transfection, using Western blot analysis. As shown in Fig. 4A, the gene knockdown was efficient and specific, producing a ~3-fold reduction in protein band intensity for HGPRT, NAMPT or ADK. The anti-APRT antibody produced several aspecific bands (data not shown), making it impossible to estimate

Molecular Pharmacology Fast Forward. Published on August 1, 2013 as DOI: 10.1124/mol.113.087247
This article has not been copyedited and formatted. The final version may differ from this version.

the APRT gene knockdown efficiency by Western blot. We therefore did an additional experiment to determine whether the cytostatic activity of the APRT-dependent 2,6-diaminopurine was altered after transfection of HEK293T cells with APRT-targeting siRNA, and we included the HGPRT-dependent compound 6-thioguanine as a control. In the APRT-siRNA condition, the IC_{50} value for 2,6-diaminopurine was ~1.8-fold increased compared to the IC_{50} value obtained in non-siRNA-transfected control cells (condition CC in Fig. 4B). For 6-thioguanine, no difference in IC_{50} value was seen among the three siRNA- and non-transfected conditions. This may be explained by the fact that 6-thioguanine is a very efficient substrate for HGPRT, since its k_{cat}/K_m value is 5.1 $s^{-1}.\mu M^{-1}$, which is similar to the value for guanine (4.3 $s^{-1}.\mu M^{-1}$). Hence, a 3-fold reduction in expression of the HGPRT enzyme (as evidenced by our Western blot analysis; Fig. 4A) appears not to be sufficient to alter the cytostatic effect of 6-thioguanine. On the other hand, the conversion of 2,6-diaminopurine by APRT was reported to be 10-fold less efficient than that of adenine (Thomas et al., 1973), explaining the decreased cytostatic activity of 2,6-daminopurine after APRT-specific gene knockdown.

The effect of the siRNA-mediated gene knockdown on the anti-vRNP activity of T-705, T-1105 and ribavirin is presented in Table 4 and Fig. 4C. After knockdown for HGPRT, the EC_{50} values for suppression of influenza virus vRNP were significantly ($P < 0.01$) increased, i.e. 8- and 5-fold for T-705 and T-1105, respectively, when compared to the EC_{50} values in the non-siRNA-treated cell control. The other siRNA treatments (including those for APRT and NAMPT) had no effect on the EC_{50} values of T-705 and its non-fluorinated analogue. In the case of ribavirin, a significant ($P < 0.05$) 6-fold increase in EC_{50} value was seen after gene knockdown for ADK, whereas its EC_{50} value was unaltered after gene knockdown for HGPRT, APRT or NAMPT.

Molecular Pharmacology Fast Forward. Published on August 1, 2013 as DOI: 10.1124/mol.113.087247
This article has not been copyedited and formatted. The final version may differ from this version.

Substrate efficiency of T-705 for human HGPRT and APRT

The above data provide strong evidence that T-705 and T-1105 require phosphoribosylation by mammalian HGPRT to exert their anti-influenza virus effect, whereas APRT and NAMPT appear not to be involved. The substrate efficiency of T-705 and T-1105 for conversion by HGPRT was investigated in enzymatic assays with human HGPRT, using UV-HPLC analysis to separate and quantify the base and ribose 5′-monophosphate (RMP) metabolite. The naturally occurring HGPRT substrates guanine and hypoxanthine (at a concentration of 8 μM) were 90-100% converted to GMP and IMP, respectively, after 30 min incubation in the presence of 200 μM *P*Rib-*PP* and 0.019 μM enzyme [hereafter referred to as 'condition A']. At these substrate concentrations, V_{max} for the reaction will have been achieved since the K_m^{app} values for guanine, hypoxanthine and *P*Rib-*PP* are 1.9, 3.4 and 65 μM, respectively. Under these assay conditions, no conversion of T-705 (at a concentration of 200 μM) was observed, even after 24 h. When exposing the compound to a 20-fold higher concentration of enzyme (i.e. 0.37 μM) and a 35-fold higher concentration of *P*Rib-*PP* (i.e. 7 mM) ('condition B'), T-705-RMP was already formed after 1 hour incubation, and its peak area linearly increased in time until 24 h incubation, the last time point measured (Fig. 5A). 'Condition B' was used in subsequent experiments to estimate the K_m^{app} values for T-705 and T-1105, using an incubation time of 6 h. The reaction velocity increased with compound concentration (Fig. 5B), yet saturation of the Michaelis-Menten curve was not obtained at 5 mM, the highest concentration attainable due to restricted compound solubility and percentage DMSO allowed. However, the data allowed to calculate estimated K_m^{app} values of 6.4 mM for T-705 and 4.1 mM for T-1105, and catalytic efficiency (k_{cat}/K_m^{app}) values of 0.000027 and 0.00014 $s^{-1}.\mu M^{-1}$, respectively. A parallel experiment with hypoxanthine and guanine under 'condition A' yielded a K_m^{app} value of 3.6 μM for hypoxanthine and 5.4 μM for guanine, which is similar to published data (Keough et al., 2006;Raman et al., 2004). The k_{cat}/K_m^{app} values were

Molecular Pharmacology Fast Forward. Published on August 1, 2013 as DOI: 10.1124/mol.113.087247
This article has not been copyedited and formatted. The final version may differ from this version.

calculated to be 0.13 $s^{-1}.\mu M^{-1}$ for hypoxanthine and 0.14 $s^{-1}.\mu M^{-1}$ for guanine, which is 12- to 32-fold lower than published values (Keough et al., 2006). Hence, it is possible that the k_{cat}/K_m^{app} values calculated for T-705 and T-1105 may be somewhat underestimated. However, our data clearly demonstrate that T-705 and T-1105 are both poor substrates of HGPRT under steady-state conditions, although the non-fluorinated compound still performs 5-fold better in terms of catalytic efficiency. This is also evident from our findings that, after 6 h incubation of the HGPRT enzyme with 5 mM T-705 or T-1105, there is still 88% of parent T-705 and 50% of T-1105 left. We further found that unsubstituted 2-pyrazinecarboxamide and 6-chloro-3,5-diamino-2-pyrazinecarboxamide were not detectably converted by HGPRT (data not shown), indicating that the 3-hydroxyl function present in T-705 and T-1105 is critical for their substrate recognition by HGPRT.

Due to the absence of external standards of the RMP metabolites of T-705 and T-1105, additional experiments were performed to confirm their peak identity on our chromatograms. A first indication that these peaks represented T-705-RMP and T-1105-RMP came from their high retention time (12.1 min in both cases) on an anion-exchange column. Secondly, samples obtained after 24 h incubation of T-705 or T-1105 with HGPRT (to form considerable amounts of the presumed RMP metabolites) were incubated with alkaline phosphatase at pH 8.5 during 60 min, and then submitted to HPLC analysis. The phosphatase treatment resulted in a total loss of the presumed T-705-RMP peak as evidenced by anion-exchange HPLC, and reverse-phase analysis revealed the formation of a new metabolite with a retention time of 21.5 min and a λ_{max} of 372 nm; for parent T-705, the respective data were 22.0 min and 320 nm. In the case of T-1105, the new metabolite had an RT of 19.8 min and λ_{max} of 348 nm, compared to 4.7 min and 348 nm for parent T-1105. This more lipophilic behaviour is consistent with the identification of the alkaline phosphatase product as ribosylated T-1105. Regarding T-705, we noticed only a 0.5 min difference in the RP-18 retention times for the

Molecular Pharmacology Fast Forward. Published on August 1, 2013 as DOI: 10.1124/mol.113.087247
This article has not been copyedited and formatted. The final version may differ from this version.

nucleobase and ribosylated metabolite. The markedly higher RT for parent T-705 compared to T-1105 (i.e. 22.0 *versus* 4.7 min) might indicate that T-705 is more lipophilic due to the presence of the fluoro at the C-6 position. Alternatively, since the elution buffer contained a negative counterion, it may mean that the basicity of T-705 is higher than that of its non-fluorinated analogue. In samples incubated with the alkaline buffer in the absence of alkaline phosphatase, the RMP metabolites were intact, indicating that the phosphate moiety was specifically removed by alkaline phosphatase.

The finding that T-705 was recognized as a substrate by HGPRT, though inefficiently, suggested that T-705 might be able to act as a competitive inhibitor of the HGPRT enzyme. Inhibition studies were performed to investigate whether T-705 inhibits the phosphoribosylation of guanine or hypoxanthine. Under the conditions tested (37 nM HGPRT; 200 µM *P*Rib-*PP*; 8 µM guanine or hypoxanthine; 10 min incubation), T-705 afforded no inhibition at 200 µM. This result is consistent with the high K_m^{app} of T-705. As a control, two acyclic nucleoside phosphonate analogues were included, which we previously found to inhibit the human HGPRT enzyme (Keough et al., 2009). 9-[(2-Phosphonoethoxy)ethyl]guanine inhibited the conversion of guanine with an IC_{50} value of 2.6 µM, whereas 9-[(2-phosphonoethoxy)ethyl]hypoxanthine displayed an IC_{50} value of 12 µM *versus* conversion of hypoxanthine.

Finally, the substrate efficiency of T-705 and T-1105 for phosphoribosylation by APRT was determined in similar experiments as performed with HGPRT. Under conditions of 0.05 mM *P*Rib-*PP* and 0.051 µM APRT enzyme, the estimated K_m^{app} of the natural substrate adenine was 14 µM. For T-705 and T-1105, evaluated under conditions of 7 mM *P*Rib-*PP* and 0.77 µM APRT enzyme, the Michaelis-Menten curve (Fig. 5C) did not reach sufficient saturation to calculate reliable values for K_m^{app}. We determined that, after 6 h incubation of the compound (at 5 mM) with APRT, only 0.3% of T-705 was converted into T-705-RMP; for T-

Molecular Pharmacology Fast Forward. Published on August 1, 2013 as DOI: 10.1124/mol.113.087247
This article has not been copyedited and formatted. The final version may differ from this version.

1105, the conversion rate was 1.2 %. For comparison, the conversion rates after 6 h incubation with HGPRT were 12% for T-705 and 50% for T-1105. Thus, it can be estimated that conversion of T-705 and T-1105 by APRT is ~40-fold less efficient compared to their phosphoribosylation by HGPRT.

T-705 is only marginally converted to its riboside by human PNP

The free RBV base was reported to be a substrate for PNP from calf spleen, resulting in the formation of ribavirin (Streeter et al., 1977). We therefore assessed whether T-705 may be recognized by the human PNP enzyme. With hypoxanthine as the substrate (at 100 µM), conversion into inosine was 99% after 30 min incubation with 0.0029 µM human PNP and 1 mM ribose-1-phosphate. Using a 20-fold higher enzyme concentration (0.058 µM), 7 mM ribose-1-phosphate and a T-705 concentration of 5 mM, conversion of T-705 into its ribosylated form was 0% after 6 h and 9% after 24 h. For T-1105, the conversion rate was 0% after 6 h and 4% after 24 h (data not shown).

Crystal structure of human HGPRT in complex with T-705-RMP

The crystal structure of T-705-RMP in complex with human HGPRT has been determined to 2.7 Å resolution, with the asymmetric unit constituting a single polypeptide of human HGPRT (Table 5). The overall fold is similar to that of the GMP.human HGPRT complex (Eads et al., 1994). This is as expected as both T-705-RMP and GMP are phosphoribosylated products of the HGPRT reaction. In order to ensure that the electron density in the active site could be attributed to the presence of T-705-RMP, we also grew crystals of human HGPRT where the only additives were DMSO (5%) and *P*Rib-*PP* (7.2 mM). No electron density in the active site was observed.

Molecular Pharmacology Fast Forward. Published on August 1, 2013 as DOI: 10.1124/mol.113.087247
This article has not been copyedited and formatted. The final version may differ from this version.

The pyrazine ring of T-705-RMP slots in neatly under the side chain of Phe186 (Fig. 6A). However, the usual π-stacking arrangement found when a purine base binds to human HGPRT is not observed here (Shi et al., 1999;Eads et al., 1994;Keough et al., 2013;Keough et al., 2009). This is a result of the carboxamide group in T-705 being more bulky than the 6-oxo group in the naturally-occurring base substrates (Fig. 6B). The pyrazine ring of T-705 is stabilized by a hydrogen bond between its exocyclic amide and the main chain carbonyl of Val187; a halogen bond between its fluorine atom, the carbonyl atom of Asp193, and the amide nitrogen of Asp193; and by the carboxamide oxygen atom of T-705 forming hydrogen bonds with the carboxyl function of Asp137 and the NZ atom of Lys165 (Fig. 6A). This interaction with Lys165 probably explains why T-705 is recognized as a substrate by human HGPRT, since this bond is analogous to the interaction between Lys165 and the 6-oxo atom of the naturally occurring purine substrates (i.e. guanine and hypoxanthine). This 6-oxo atom confers the specificity of human HGPRT for these substrates, since purine bases containing a 6-amino group (i.e. adenine) are no substrates for HGPRT.

The phosphoryl oxygens of T-705-RMP are located in the 5′-phosphate binding pocket (residues 137-141) (Fig. 6A). These atoms form hydrogen bonds with the main chain amide atoms of residues Thr138, Gly139 and Thr141, and the OG1 atom of Thr141. There are no magnesium ions in the T-705-RMP.HGPRT crystal structure. This is also the case when a nucleoside-5′-monophosphate binds. It is assumed that the divalent metal ions exit with PP_i. The interactions of the 2′- and 3′-hydroxyl groups of the ribose ring of T-705-RMP with the NZ atom of Lys68 are unique and, until now, only observed with this ligand. Also, in the T-705-RMP complex, the side chain of residue Lys68 adopts a different orientation from that seen when GMP is bound (Fig. 6B). In the case of T-705-RMP, the two (i.e. 2′- and 3′-) hydroxyl groups of the ribose form hydrogen bonds with the NZ atom of Lys68 (Fig. 6A). The side chain of Lys68 is only found in this position in four other known crystal structures of

Molecular Pharmacology Fast Forward. Published on August 1, 2013 as DOI: 10.1124/mol.113.087247
This article has not been copyedited and formatted. The final version may differ from this version.

human HGPRT (Keough et al., 2009;Keough et al., 2005). The common feature of these structures is the absence of PP_i or a mimic thereof. When the transition state analogue immucillinGP binds along with $PP_i.Mg^{2+}$ (Shi et al., 1999), or when {[(2-[(guanine-9*H*-yl)methyl]propane-1,3-diyl)bis(oxy)]bis(methylene)}diphosphonic acid binds (Keough et al., 2013), the side chain of Lys68 rotates away from the active site by 180^o to allow $PP_i.Mg^{2+}$ to enter. In the immucillin.GP complex, the ribose is coordinated to Mg^{2+} and through this to PP_i (Shi et al., 1999). One of its hydroxyl groups also forms a hydrogen bond with the OE1 atom of Glu133. Instead, in the T-705-RMP structure, the OE1 atom of Glu133 forms a hydrogen bond with the NZ of Lys68. In the GMP.HGPRT co-crystal complex, the side chain of Lys68 is orientated away from Glu133. It has been hypothesized that, in that structure, this side chain is returning to its original position prior to release of the nucleoside-5′-monophosphate. The crystal structure with T-705-RMP may reflect the active site structure prior to nucleotide release, since T-705-RMP has been captured in the crystal before it can be released. This suggests that T-705-RMP may have a relatively high affinity for the enzyme with a K_i value well below the K_m^{app} value for T-705, or else catalysis would not occur.

Molecular Pharmacology Fast Forward. Published on August 1, 2013 as DOI: 10.1124/mol.113.087247
This article has not been copyedited and formatted. The final version may differ from this version.

DISCUSSION

T-705 is unique in having broad anti-RNA virus activity, favourable selectivity and a high resistance barrier (Furuta et al., 2009). Due to its rotating carboxamide, T-705 acts as a pseudobase mimicking both guanine and adenine. This is the likely basis for recognition of T-705 and its metabolites by cellular enzymes involved in purine metabolism. Likewise, the influenza virus polymerase recognizes T-705-RTP as a GTP-mimic, giving competitive inhibition of GTP incorporation during viral RNA synthesis (Furuta et al., 2005). The increased mutation rate in influenza virus passaged under T-705 (Baranovich et al., 2013) is explained by the presumption that, once incorporated into viral RNA, T-705 can base-pair with either cytosine or uracil. Thus, both the metabolic activation and antiviral effect of T-705 depend on the equilibrium between its guanine *versus* adenine mimicking rotamer. We here demonstrate that, for its initial activation consisting of phosphoribosylation, T-705 behaves more as a mimic of guanine than of adenine. Our enzymatic data indicate that its conversion by HGPRT is about 40-fold more efficient compared to that by APRT.

The guanine mimicking property of T-705 was confirmed in the T-705-RMP.HGPRT crystal structure, in which the carbonyl oxygen of its carboxamide interacts with Lys165, similar as the 6-oxo atom of the natural purine substrates (Eads et al., 1994). A second similarity between the co-crystal structures with T705-RMP or GMP is the interaction of their 5′-phosphate with the loop formed by residues 137-141. On the other hand, the low binding affinity of T-705 compared to guanine (i.e. ~1200-fold lower K_m^{app} value) may be explained by the different location of the aromatic ring in relation to the side chain of Phe186 (Fig. 6B). With GMP, π-stacking between Phe186 and the purine ring is observed. In the case of T-705-RMP, the pyrazine ring is close to the aromatic ring of Phe186, which is however slightly pushed away by the bulky carboxamide group. Also, hydrogen bonds are formed with Val187 and Lys165. Though these bonds contribute to the binding of T-705 in the active site, they

Molecular Pharmacology Fast Forward. Published on August 1, 2013 as DOI: 10.1124/mol.113.087247
This article has not been copyedited and formatted. The final version may differ from this version.

may be counter-productive. The free rotation around the carbon-carbon bond, which allows the carbonyl and amide groups to adopt different positions, may contribute to the high K_m^{app} value of T-705. In comparison, the 6-oxogroup of guanine is fixed and ready to form a hydrogen bond with Lys165, thereby positioning the base in the perfect position. Due to its high K_m^{app} value, the catalytic efficiency (k_{cat}/K_m) for conversion of T-705 by HGPRT is low. However, its turnover number seems reasonable, since its k_{cat} was estimated to be 0.17 s^{-1} compared to 0.74 s^{-1} for guanine.

In the crystal structure with T-705-RMP, the 6-fluorine forms halogen bonds with residue Asp193 (Fig. 6A). With the non-fluorinated analogue T-1105, this same interaction cannot occur, and hence its pyrazine ring may adopt a somewhat different orientation, resulting in a slightly (1.5-fold) lower K_m^{app} value and a 3-fold higher k_{cat} value. The crystal structure cannot explain why 2-pyrazinamide is not a substrate for HGPRT. The absence of the 3-hydroxyl may disturb the electronic configuration, so that the nitrogen atom becomes a weaker nucleophile and catalysis cannot proceed. Thus, whereas the 3-hydroxyl function of T-705 is critical for recognition by HGPRT, its 6-fluoro atom is not required for metabolic activation and antiviral activity. T-1105 is converted 5-fold more efficiently by human HGPRT and, likewise, proved 4-fold more potent than T-705 in influenza virus-infected MDCK cells. However, T-1105 was ~14-fold less active in HEK293T cells than in MDCK cells; for T-705, the EC_{50} values were similar in both cell lines. This discrepancy may be related to a different efficiency between MDCK and HEK293T cells in performing the activation beyond the RMP metabolites. The enzymes involved are not yet identified but a role for GMP kinase and NDP kinase is possible. Whether the difference is related to species (MDCK are of canine origin while HEK293T cells are human) or cell line-dependent expression of the activating enzymes is not clear. In African green monkey Vero cells, T-705 was ~3-fold more active against parainfluenza-3 virus and Punta Toro virus compared to T-1105 (data not shown).

Molecular Pharmacology Fast Forward. Published on August 1, 2013 as DOI: 10.1124/mol.113.087247
This article has not been copyedited and formatted. The final version may differ from this version.

Conversely, T-1105 proved more potent than T-705 when evaluated against foot-and-mouth disease virus in pig cells (Sakamoto et al., 2006). Thus, the antiviral outcome of these broad acting 2-pyrazinecarboxamide derivatives is not only governed by recognition of their RTP metabolites by the given viral polymerase, since their species-dependent activation is equally important.

The complete lack of antiviral activity of T-705 and T-1105 in HGPRT-deficient MDCK cells unambiguously proves that HGPRT is required for their activation. This is also evident from our gene knockdown experiments, which further revealed that two other phosphoribosyltransferases, APRT and NAMPT, are irrelevant for the antiviral activity of these 2-pyrazinecarboxamide compounds. NAMPT was included because of the structural analogy between T-705 and nicotinamide (Burgos et al., 2009). These gene knockdown experiments confirmed the role for ADK in activating ribavirin (Willis et al., 1978).

At first sight, the absolute HGPRT dependency may disagree with the low efficiency for phosphoribosylation of T-705 and T-1105 in the enzymatic assays with human HGPRT. We estimated their K_m^{app} values to be 6.4 and 4.1 mM, respectively. Their catalytic efficiency was 4700-fold (for T-705) and 900-fold (for T-1105) lower compared to that of the natural substrate hypoxanthine. Our conclusion that the HGPRT reaction is a rate-limiting step in the activation of T-705 agrees with reported cell culture metabolism data (Furuta et al., 2005), since the MDCK cells contained high amounts of T-705 but lower amounts of its RMP and RTP metabolites. However, steady-state enzymatic assays may not fully predict the dynamic conversion of nucleoside analogues in cell culture. For instance, the K_m^{app} value of ribavirin for ADK was reported to be 0.54 or 7.8 mM (depending on the buffer conditions) (Wu et al., 2005), and yet, ADK does have a critical role in activation of ribavirin (Willis et al., 1978). Also, it has been documented that a K_m^{app} value in the millimolar range does not exclude an efficient antiviral outcome since didanosine, a potent anti-HIV compound, is

Molecular Pharmacology Fast Forward. Published on August 1, 2013 as DOI: 10.1124/mol.113.087247
This article has not been copyedited and formatted. The final version may differ from this version.

monophosphorylated by 5′-nucleotidase at a substrate affinity in the lower millimolar range (Johnson and Fridland, 1989).

A concern in antiviral therapy with nucleoside analogues is that suboptimal levels of the active metabolite may precipitate the emergence of drug resistance. This may be different for T-705 since, at lower concentrations, its incorporation into viral RNA can cause lethal mutagenesis and virus extinction (Baranovich et al., 2013). In cell culture, no T-705 resistant influenza virus was detected after as many as thirty passages (Furuta et al., 2009). T-705 is a broad antiviral agent applicable for the treatment of various viral disease manifestations (Furuta et al., 2009). Since HGPRT is a ubiquitous enzyme, T-705 should become phosphoribosylated in all relevant tissues. Its HGPRT-dependency may be an interesting property in the treatment of neurological virus infections, since the expression of HGPRT is 4-fold higher in brain (Stout and Caskey, 1985). This is consistent with the severe neurological abnormalities in Lesch-Nyhan patients who have a congenital HGPRT deficiency (Jinnah et al., 2000). Although HGPRT-deficient cells display normal proliferation *in vitro* (due to unaffected purine *de novo* synthesis), HGPRT is indispensable *in vivo*. The level of HPRT1 mRNA was found to be reduced in inflamed lung tissue (Allen et al., 2006). No data have yet been reported on the tissue distribution or metabolism of T-705 *in vivo*. Besides T-705, the ribosylated form of T-1105 is currently being developed as an antiviral agent (Furuta et al., 2009). This nucleoside analogue (encoded T-1106) appeared not active against yellow fever virus in Vero cells, but was shown to suppress this virus in a hamster model (Julander et al., 2009). In our enzymatic assays with human PNP, ribosylation of T-705 or T-1105 was very low or barely detected. Whether the reverse reaction may occur, i.e. PNP-mediated phosphorolysis of T-1106 into T-1105, is not known. The free base of ribavirin was shown to be ribosylated by PNP whereas it was not phosphoribosylated by HGPRT (Streeter et al., 1977).

Molecular Pharmacology Fast Forward. Published on August 1, 2013 as DOI: 10.1124/mol.113.087247
This article has not been copyedited and formatted. The final version may differ from this version.

The inefficient activation of T-705 and T-1105 by HGPRT could represent a drawback in terms of their eventual antiviral potency *in vivo*. The small size of the 2-pyrazinecarboxamide scaffold limits the number of modifications that could be considered to improve their activation profile. In the patent related to these antiviral agents, Furuta and Egawa (2001) described several structural analogues of T-705 and T-1105 containing, among other substitutions, a chlorine or bromine at position 6, or a different heterocycle; neither of these close analogues displayed anti-influenza virus activity. However, a well-known strategy to bypass inefficient activation of nucleoside analogues is to design lipophilic prodrugs of their monophosphate forms. These membrane-permeable prodrugs readily enter the cells and then release the active nucleoside-5′-monophosphate form by metabolic or chemical activation (Mehellou et al., 2009;Meier and Balzarini, 2006). Our studies indicate that phosphoribosylation of T-705 and T-1105 by HGPRT is rather inefficient, and hence, it seems relevant to apply the prodrug concept to these antiviral compounds to potentially increase their biodisposition and therapeutic effectiveness.

Molecular Pharmacology Fast Forward. Published on August 1, 2013 as DOI: 10.1124/mol.113.087247
This article has not been copyedited and formatted. The final version may differ from this version.

ACKNOWLEDGMENTS

The authors wish to thank Wim van Dam, Lizette van Berckelaer and Ria Van Berwaer for their dedicated technical assistance. Preliminary X-ray data were measured at the University of Queensland Remote-Operation Crystallization and X-ray diffraction facility (UQROCX). The final measurements were made at the MX1 beamline, Australian Synchrotron, Clayton, with the assistance of Alan Riboldi-Tunnicliffe and Tom Caradoc-Davies. The views expressed herein are those of the authors and not necessarily those of the owner or operator of the Australian Synchotron.

AUTHORSHIP CONTRIBUTIONS

Participated in research design: Naesens, Guddat, Keough, van Kuilenburg and Balzarini.

Conducted experiments: Naesens, Guddat, Keough, Meijer and Balzarini.

Performed data analysis: Naesens, Guddat, Keough, van Kuilenburg, Vande Voorde and Balzarini.

Wrote or contributed to the writing of the manuscript: Naesens, Guddat, Keough, van Kuilenburg, Vande Voorde and Balzarini.

Molecular Pharmacology Fast Forward. Published on August 1, 2013 as DOI: 10.1124/mol.113.087247
This article has not been copyedited and formatted. The final version may differ from this version.

Reference List

Adams PD, Afonine P V, Bunkoczi G, Chen V B, Davis I W, Echols N, Headd J J, Hung L W, Kapral G J, Grosse-Kunstleve R W, McCoy A J, Moriarty N W, Oeffner R, Read R J, Richardson D C, Richardson J S, Terwilliger T C and Zwart P H (2010) PHENIX: a Comprehensive Python-Based System for Macromolecular Structure Solution. *Acta Crystallogr D Biol Crystallogr* **66**:213-221.

Allen IC, Pace A J, Jania L A, Ledford J G, Latour A M, Snouwaert J N, Bernier V, Stocco R, Therien A G and Koller B H (2006) Expression and Function of NPSR1/GPRA in the Lung Before and After Induction of Asthma-Like Disease. *Am J Physiol Lung Cell Mol Physiol* **291**:L1005-L1017.

Baranovich T, Wong S S, Armstrong J, Marjuki H, Webby R J, Webster R G and Govorkova E A (2013) T-705 (Favipiravir) Induces Lethal Mutagenesis in Influenza A H1N1 Viruses In Vitro. *J Virol* **87**:3741-3751.

Burgos ES, Ho M C, Almo S C and Schramm V L (2009) A Phosphoenzyme Mimic, Overlapping Catalytic Sites and Reaction Coordinate Motion for Human NAMPT. *Proc Natl Acad Sci U S A* **106**:13748-13753.

Chen TR (1983) Chromosome Changes in 6-TG-Resistant Mutant Strains Derived From a Karyotypically Stable Human Line, C32. *Cytogenet Cell Genet* **35**:181-189.

Crotty S, Maag D, Arnold J J, Zhong W, Lau J Y, Hong Z, Andino R and Cameron C E (2000) The Broad-Spectrum Antiviral Ribonucleoside Ribavirin Is an RNA Virus Mutagen. *Nat Med* **6**:1375-1379.

De Bolle L, Michel D, Mertens T, Manichanh C, Agut H, De Clercq E and Naesens L (2002) Role of the Human Herpesvirus 6 U69-Encoded Kinase in the Phosphorylation of Ganciclovir. *Mol Pharmacol* **62**:714-721.

Eads JC, Scapin G, Xu Y, Grubmeyer C and Sacchettini J C (1994) The Crystal Structure of Human Hypoxanthine-Guanine Phosphoribosyltransferase With Bound GMP. *Cell* **78**:325-334.

Emsley P, Lohkamp B, Scott W G and Cowtan K (2010) Features and Development of Coot. *Acta Crystallogr D Biol Crystallogr* **66**:486-501.

Furuta Y and Egawa H (2001) Nitrogenous Heterocyclic Carboxamide Derivatives or Salts Thereof and Antiviral Agents Containing Both. Patent number EP1112743A1.

Furuta Y, Takahashi K, Fukuda Y, Kuno M, Kamiyama T, Kozaki K, Nomura N, Egawa H, Minami S, Watanabe Y, Narita H and Shiraki K (2002) In Vitro and in Vivo Activities of Anti-Influenza Virus Compound T-705. *Antimicrob Agents Chemother* **46**:977-981.

Furuta Y, Takahashi K, Kuno-Maekawa M, Sangawa H, Uehara S, Kozaki K, Nomura N, Egawa H and Shiraki K (2005) Mechanism of Action of T-705 Against Influenza Virus. *Antimicrob Agents Chemother* **49**:981-986.

Furuta Y, Takahashi K, Shiraki K, Sakamoto K, Smee D F, Barnard D L, Gowen B B, Julander J G and Morrey J D (2009) T-705 (Favipiravir) and Related Compounds: Novel Broad-Spectrum Inhibitors of RNA Viral Infections. *Antiviral Res* **82**:95-102.

Gowen BB, Wong M H, Jung K H, Sanders A B, Mendenhall M, Bailey K W, Furuta Y and Sidwell R W (2007) In Vitro and in Vivo Activities of T-705 Against Arenavirus and Bunyavirus Infections. *Antimicrob Agents Chemother* **51**:3168-3176.

Hayden F (2009) Developing New Antiviral Agents for Influenza Treatment: What Does the Future Hold? *Clin Infect Dis* **48 Suppl 1**:S3-13.

Hoffmann E, Neumann G, Kawaoka Y, Hobom G and Webster R G (2000) A DNA Transfection System for Generation of Influenza A Virus From Eight Plasmids. *Proc Natl Acad Sci U S A* **97**:6108-6113.

Jinnah HA, De G L, Harris J C, Nyhan W L and O'Neill J P (2000) The Spectrum of Inherited Mutations Causing HPRT Deficiency: 75 New Cases and a Review of 196 Previously Reported Cases. *Mutat Res* **463**:309-326.

Johnson MA and Fridland A (1989) Phosphorylation of 2',3'-Dideoxyinosine by Cytosolic 5'-Nucleotidase of Human Lymphoid Cells. *Mol Pharmacol* **36**:291-295.

Julander JG, Shafer K, Smee D F, Morrey J D and Furuta Y (2009) Activity of T-705 in a Hamster Model of Yellow Fever Virus Infection in Comparison With That of a Chemically Related Compound, T-1106. *Antimicrob Agents Chemother* **53**:202-209.

Kabsch W (2010) XDS. *Acta Crystallogr D Biol Crystallogr* **66**:125-132.

Kao RY, Yang D, Lau L S, Tsui W H, Hu L, Dai J, Chan M P, Chan C M, Wang P, Zheng B J, Sun J, Huang J D, Madar J, Chen G, Chen H, Guan Y and Yuen K Y (2010) Identification of Influenza A Nucleoprotein As an Antiviral Target. *Nat Biotechnol* **28**:600-605.

Keough DT, Brereton I M, de J J and Guddat L W (2005) The Crystal Structure of Free Human Hypoxanthine-Guanine Phosphoribosyltransferase Reveals Extensive Conformational Plasticity Throughout the Catalytic Cycle. *J Mol Biol* **351**:170-181.

Keough DT, Hockova D, Holy A, Naesens L M, Skinner-Adams T S, Jersey J and Guddat L W (2009) Inhibition of Hypoxanthine-Guanine Phosphoribosyltransferase by Acyclic Nucleoside Phosphonates: a New Class of Antimalarial Therapeutics. *J Med Chem* **52**:4391-4399.

Keough DT, Skinner-Adams T, Jones M K, Ng A L, Brereton I M, Guddat L W and de J J (2006) Lead Compounds for Antimalarial Chemotherapy: Purine Base Analogs Discriminate Between Human and P. Falciparum 6-Oxopurine Phosphoribosyltransferases. *J Med Chem* **49**:7479-7486.

Keough DT, Spacek P, Hockova D, Tichy T, Vrbkova S, Slavetinska L, Janeba Z, Naesens L, Edstein M D, Chavchich M, Wang T H, de J J and Guddat L W (2013) Acyclic Nucleoside Phosphonates Containing a Second Phosphonate Group Are Potent Inhibitors of 6-Oxopurine Phosphoribosyltransferases and Have Antimalarial Activity. *J Med Chem* **56**:2513-2526.

Kiso M, Takahashi K, Sakai-Tagawa Y, Shinya K, Sakabe S, Le Q M, Ozawa M, Furuta Y and Kawaoka Y (2010) T-705 (Favipiravir) Activity Against Lethal H5N1 Influenza A Viruses. *Proc Natl Acad Sci U S A* **107**:882-887.

Martinez-Sobrido L and Garcia-Sastre A (2010) Generation of Recombinant Influenza Virus From Plasmid DNA. *J Vis Exp* 2057.

Masino SA, Li T, Theofilas P, Sandau U S, Ruskin D N, Fredholm B B, Geiger J D, Aronica E and Boison D (2011) A Ketogenic Diet Suppresses Seizures in Mice Through Adenosine A(1) Receptors. *J Clin Invest* **121**:2679-2683.

McCoy AJ, Grosse-Kunstleve R W, Adams P D, Winn M D, Storoni L C and Read R J (2007) Phaser Crystallographic Software. *J Appl Crystallogr* **40**:658-674.

Mehellou Y, Balzarini J and McGuigan C (2009) Aryloxy Phosphoramidate Triesters: a Technology for Delivering Monophosphorylated Nucleosides and Sugars into Cells. *ChemMedChem* **4**:1779-1791.

Meier C and Balzarini J (2006) Application of the CycloSal-Prodrug Approach for Improving the Biological Potential of Phosphorylated Biomolecules. *Antiviral Res* **71**:282-292.

Meneghesso S, Vanderlinden E, Brancale A, Balzarini J, Naesens L and McGuigan C (2013) Synthesis and Biological Evaluation of Purine 2'-Fluoro-2'-Deoxyriboside ProTides As Anti-Influenza Virus Agents. *ChemMedChem* **8**:415-425.

Morrey JD, Taro B S, Siddharthan V, Wang H, Smee D F, Christensen A J and Furuta Y (2008) Efficacy of Orally Administered T-705 Pyrazine Analog on Lethal West Nile Virus Infection in Rodents. *Antiviral Res* **80**:377-379.

Moscona A (2008) Medical Management of Influenza Infection. *Annu Rev Med* **59**:397-413.

Moscona A (2009) Global Transmission of Oseltamivir-Resistant Influenza. *N Engl J Med* **360**:953-956.

Osterhaus A, Fouchier R and Rimmelzwaan G (2011) Towards Universal Influenza Vaccines? *Philos Trans R Soc Lond B Biol Sci* **366**:2766-2773.

Raman J, Sumathy K, Anand R P and Balaram H (2004) A Non-Active Site Mutation in Human Hypoxanthine Guanine Phosphoribosyltransferase Expands Substrate Specificity. *Arch Biochem Biophys* **427**:116-122.

Rocha-Pereira J, Jochmans D, Dallmeier K, Leyssen P, Nascimento M S and Neyts J (2012) Favipiravir (T-705) Inhibits in Vitro Norovirus Replication. *Biochem Biophys Res Commun* **424**:777-780.

Sakamoto K, Ohashi S, Yamazoe R, Takahashi K and Furuta Y. The Inhibition of FMD Virus Excretion From the Infected Pigs by an Antiviral Agent, T-1105. FAO Report of the Research Group of the Standing Technical Committee of European Commission for the control of Foot-and-Mouth Disease, Paphos, Cyprus. *FAO Report* **Appendix 64**, 418-424.

Schuttelkopf AW and van Aalten D M (2004) PRODRG: a Tool for High-Throughput Crystallography of Protein-Ligand Complexes. *Acta Crystallogr D Biol Crystallogr* **60**:1355-1363.

Shi W, Li C M, Tyler P C, Furneaux R H, Grubmeyer C, Schramm V L and Almo S C (1999) The 2.0 A Structure of Human Hypoxanthine-Guanine Phosphoribosyltransferase in Complex With a Transition-State Analog Inhibitor. *Nat Struct Biol* **6**:588-593.

Sidwell RW, Barnard D L, Day C W, Smee D F, Bailey K W, Wong M H, Morrey J D and Furuta Y (2007) Efficacy of Orally Administered T-705 on Lethal Avian Influenza A (H5N1) Virus Infections in Mice. *Antimicrob Agents Chemother* **51**:845-851.

Sleeman K, Mishin V P, Deyde V M, Furuta Y, Klimov A I and Gubareva L V (2010) In Vitro Antiviral Activity of Favipiravir (T-705) Against Drug-Resistant Influenza and 2009 A(H1N1) Viruses. *Antimicrob Agents Chemother* **54**:2517-2524.

Smee DF, Hurst B L, Egawa H, Takahashi K, Kadota T and Furuta Y (2009) Intracellular Metabolism of Favipiravir (T-705) in Uninfected and Influenza A (H5N1) Virus-Infected Cells. *J Antimicrob Chemother* **64**:741-746.

Stevaert A, Dallocchio R, Dessi A, Pala N, Rogolino D, Sechi M and Naesens L (2013) Mutational Analysis of the Binding Pockets of the Diketo Acid Inhibitor L-742,001 in the Influenza Virus PA Endonuclease. *J Virol* Epub ahead of print.

Stout JT and Caskey C T (1985) HPRT: Gene Structure, Expression, and Mutation. *Annu Rev Genet* **19**:127-148.

Streeter DG, Miller J P, Robins R K and Simon L N (1977) The Enzymic Conversion of 1,2,4-Triazole-3-Carboxamide to Ribavirin-5'-Phosphate and Its Relationship to the Proposed Mechanism of Action. *Ann N Y Acad Sci* **284**:201-210.

Thomas CB, Arnold W J and Kelley W N (1973) Human Adenine Phosphoribosyltransferase. Purification, Subunit Structure, and Substrate Specificity. *J Biol Chem* **248**:2529-2535.

Vanderlinden E, Goktas F, Cesur Z, Froeyen M, Reed M L, Russell C J, Cesur N and Naesens L (2010) Novel Inhibitors of Influenza Virus Fusion: Structure-Activity Relationship and Interaction With the Viral Hemagglutinin. *J Virol* **84**:4277-4288.

Vanderlinden E, Vanstreels E, Boons E, ter Veer W, Huckriede A, Daelemans D, Van Lommel A, Roth E, Sztaricskai F, Herczegh P and Naesens L (2012) Intracytoplasmic Trapping of Influenza Virus by a Lipophilic Derivative of Aglycoristocetin. *J Virol* **86**:9416-9431.

Willis RC, Carson D A and Seegmiller J E (1978) Adenosine Kinase Initiates the Major Route of Ribavirin Activation in a Cultured Human Cell Line. *Proc Natl Acad Sci U S A* **75**:3042-3044.

Wu JZ, Larson G, Walker H, Shim J H and Hong Z (2005) Phosphorylation of Ribavirin and Viramidine by Adenosine Kinase and Cytosolic 5'-Nucleotidase II: Implications for Ribavirin Metabolism in Erythrocytes. *Antimicrob Agents Chemother* **49**:2164-2171.

Molecular Pharmacology Fast Forward. Published on August 1, 2013 as DOI: 10.1124/mol.113.087247
This article has not been copyedited and formatted. The final version may differ from this version.

FOOTNOTE

This study was supported by a grant from the Geconcerteerde Onderzoeksacties [GOA/10/014] from the KU Leuven and funds from the National Health and Medical Research Council [Grant No. 1030353]. Johan Vande Voorde acknowledges a PhD grant from the Institute for the Promotion of Innovation through Science and Technology in Flanders (IWT-Vlaanderen).

Molecular Pharmacology Fast Forward. Published on August 1, 2013 as DOI: 10.1124/mol.113.087247
This article has not been copyedited and formatted. The final version may differ from this version.

FIGURE LEGENDS

Fig. 1. Chemical structures of T-705, ribavirin and structural analogues.

Fig. 2. Possible routes for conversion of T-705 or its non-fluorinated analogue T-1105 into their ribomonophosphorylated (RMP) metabolites.

This may be performed in one step by HGPRT or APRT, or in two steps, i.e. by PNP-catalyzed ribose coupling followed by a kinase-dependent phosphorylation. The dashed line shows the phosphatase reaction which was used to identify the RMP metabolites. In the left inset, the two rotational isomers of the 2-pyrazinecarboxamide compounds are shown to explain their guanine and adenine mimicking properties.

Fig. 3. Characterization of the HGPRT-deficient MDCK-TG^{res} cells.

MDCK cells were passaged in up to 200 µM 6-thioguanine, and surviving cells were expanded and subcloned. One clone, designated MDCK-TG^{res}, was characterized by genotypic and phenotypic analysis. **(A)** Western blot result showing absence of the HGPRT protein band (24 kDa) in the MDCK-TG^{res} cells. The antibody recognizes a C-terminal epitope of HGPRT. Equal protein loading for MDCK-TG^{res} and wild-type MDCK cells (MDCK-WT) cells was verified by detection of β-actin (47 kDa). **(B)** cDNA analysis of exon 1-3 of HPRT1 in MDCK and MDCK-TG^{res} cells. The 461-bp band represents the normal fragment, whereas the 354-bp cDNA fragment is 107 bp shorter due to exon-2 skipping. **(C)** Reduced incorporation of [2,8-^{3}H]Hx into purine nucleotide pools and nucleic acids of MDCK-TG^{res} cells, compared to MDCK-WT cells. After incubating the cells with 0.027 µM

Molecular Pharmacology Fast Forward. Published on August 1, 2013 as DOI: 10.1124/mol.113.087247
This article has not been copyedited and formatted. The final version may differ from this version.

[2,8-^{3}H]Hx during 24 h, cell extracts were analyzed by HPLC to determine the radioactivity incorporated into purine nucleotide pools. Incorporation into nucleic acids was measured by analysis of the methanol-insoluble fraction. Data are the mean ± S.E.M. of two independent tests.

Fig. 4. Effect of siRNA knockdown on the inhibitory activity of T-705, T-1105 and ribavirin against influenza virus polymerase.

(A) Western blot analysis to verify the gene knockdown efficiency after transfection of HEK293T cells with siRNA specific for HGPRT, ADK, APRT or NAMPT, or a negative control (NC) siRNA. CC, non-siRNA-treated cell control. Cell extracts were made at 48 h after siRNA transfection and analyzed with antibodies specific for: HGPRT, NAMPT, ADK, or β-actin (loading control). Results are not shown for the anti-APRT staining (which gave several aspecific bands). Data shown are from one representative experiment (N=2). (**B**) The efficiency of siRNA-mediated knockdown for HGPRT and APRT was also verified by determining the cytostatic activity of 2,6-diaminopurine and 6-thioguanine. At 24 h after transfection with siRNA for HGPRT, APRT or NC, the cells were trypsinized and transferred to plates containing 2,6-diaminopurine or 6-thioguanine. The IC_{50} values (concentrations producing 50% inhibition of cell proliferation) were determined 48h later. Data are the mean (± S.E.M.) increase in IC_{50} value *versus* non-siRNA-treated control cells (CC) (N=3). **(C)** Effect of siRNA-mediated gene knockdown on the EC_{50} values of T-705, T-1105, ribavirin and nucleozin in the influenza virus vRNP reconstitution assay. HEK293T cells were transfected with siRNA for the indicated genes (NC, negative control) and incubated during 48 h. The cells were then trypsinized, transfected with the influenza vRNP reconstituting and firefly luciferase reporter plasmid, and incubated with the test compounds. The luciferase activity was assessed 24 h later to determine the EC_{50}, i.e. compound concentration giving

Molecular Pharmacology Fast Forward. Published on August 1, 2013 as DOI: 10.1124/mol.113.087247
This article has not been copyedited and formatted. The final version may differ from this version.

50% reduction in firefly luciferase signal. On the Y-axis, the fold increase in EC_{50} is shown *versus* non-siRNA-treated control cells (CC). Data are the mean ± S.E.M. of 3-5 tests.

Fig. 5. Steady-state kinetics for phosphoribosylation of T-705 and T-1105 by human HGPRT or APRT.

Assay conditions: 7 mM PRPP and 0.37 µM HGPRT or 0.77 µM APRT. Panel A: HGPRT-mediated formation of T-705-RMP or T-1105-RMP as a function of incubation time (last measured time point: 24 h). Panels B and C: Michaelis-Menten curves for conversion of T-705 or T-1105 by HGPRT (panel B) or APRT (panel C) Data are the mean ± S.E.M. (N=3 in panels A and B and N=1 or 2 in panel C). In the case of HGPRT, the K_m^{app} and k_{cat}/K_m^{app} values could be estimated (see Table below panel B). Note the 40-fold difference in the Y-axis between panels B and C.

Figure 6. **Crystal structure of the complex between human HGPRT and T-705-RMP and comparison with the GMP.human HGPRT structure.** (**A**) To obtain the crystal complex with T-705-RMP, *P*Rib-*PP* and T-705 were added to human HGPRT under the conditions described in Materials and Methods. Crystallization of this solution resulted in the appearance of the nucleotide product bound in the active site of the enzyme. (**B**) Superimposition of the active site of the T-705-RMP.human HGPRT complex and the GMP.human HGPRT complex (PDB code 1HMP) (Eads et al., 1994). The atoms of the 5´-phosphate groups superimpose to a high degree of precision. The ribose ring of T-705-RMP is slightly lower in the active site compared to GMP. This difference appears to attract the side chain of K68 allowing hydrogen bond formation (shown in panel A). The pyrazine ring of T-705-RMP is lower in the purine binding site than is the guanine of GMP. As a result, in the

Molecular Pharmacology Fast Forward. Published on August 1, 2013 as DOI: 10.1124/mol.113.087247
This article has not been copyedited and formatted. The final version may differ from this version.

case of T-705-RMP, there is a reduction in π-electron overlap between the nucleotide product and the aromatic ring of F186. This dissimilarity, together with the different hydrogen bonding arrangements, may be contributing factors to the lower binding affinity of T-705 compared to that of guanine.

TABLE 1. Broad anti-influenza virus activity of T-705 and related carboxamide analogues in MDCK-WT cells.

Compound	Antiviral EC_{50} (μM)[a]						Cytotoxicity (μM)	
	Influenza A/H1N1		Influenza A/H3N2		Influenza B			
	CPE	MTS	CPE	MTS	CPE	MTS	MCC[b]	CC_{50}[c]
T-705	12 ± 1	14 ± 2	9.4 ± 0.3	12 ± 2	9.3 ± 0.4	7.2 ± 1.4	>500	>500
T-1105	3.4 ± 1.4	3.5 ± 0.6	2.8 ± 1.0	1.8 ± 0.2	3.7 ± 1.6	1.3 ± 0.0	>500	>500
2-Pyrazinamide	>500	>500	>500	>500	>500	>500	>500	>500
6-Cl-3,5-diamino-2-pyrazinamide	>500	>500	>500	>500	>500	>500	≥500	≥500
Ribavirin base	>500	>500	>500	>500	>500	>500	>500	>500
Ribavirin	9.6 ± 0.5	18 ± 5	9.6 ± 0.5	12 ± 5	15 ± 6	16 ± 7	100	>100
Nucleozin	0.017 ± 0.010	0.024 ± 0.018	0.18 ± 0.07	0.13 ± 0.04	>100	>100	15 ± 3	41 ± 16

[a]EC_{50}: compound concentration causing 50% reduction in virus replication at 72 h p.i., as estimated by the microscopic CPE reduction assay or the MTS cell viability assay.
[b]MCC: minimum cytotoxic concentration, or compound concentration causing minimal changes in cell morphology after 72 h incubation with compound.
[c]CC_{50}: 50% cytotoxic concentration, i.e. compound concentration causing 50% reduction in cell viability, as estimated by the MTS assay.
Influenza virus strains used: A/PR/8/34 (A/H1N1); A/HK/7/87 (A/H3N2); and B/HK/5/72.
Data are the mean ± S.E.M. of 3-5 independent tests.

TABLE 2. Sensitivity of WT- and HGPRT-deficient MDCK cells to diverse cytostatic agents

Compound	IC_{50} (μM)[a]	
	MDCK-WT	MDCK-TG^{res}
6-Thioguanine	8.1 ± 2.9	>500
6-Thioguanosine	1.3 ± 0.0	442 ± 81
6-Mercaptopurine	8.4 ± 1.1	>500
2,6-Diaminopurine	10 ± 2	11 ± 2
6-Methylpurine	4.2 ± 0.4	3.1 ± 0.6
Ribavirin	8.9 ± 0.2	3.4 ± 0.4
Tubercidin	0.13 ± 0.04	0.11 ± 0.06
Pyrazofurin	0.48 ± 0.58	0.31 ± 0.22
Cytarabine	1.9 ± 0.0	1.2 ± 0.2
Gemcitabine	0.090 ± 0.003	0.079 ± 0.024
5-Fluorouracil	0.073 ± 0.021	0.082 ± 0.025
5-Fluoro-2'-deoxyuridine	0.0058 ± 0.0017	0.0063 ± 0.0030
5-Trifluorothymidine	1.0 ± 0.5	1.8 ± 0.2

[a]IC_{50}: concentration causing 50% inhibition of cell proliferation.
Data are the mean ± S.E.M. of two independent tests.
Activating enzymes: HGPRT for 6-thioguanine and 6-mercaptopurine; APRT for 2,6-diaminopurine and 6-methylpurine; ADK for ribavirin, tubercidin and pyrazofurin; 2'-deoxycytidine kinase for cytarabine and gemcitabine, orotate phosphoribosyltransferase or thymidine phosphorylase for 5-fluorouracil; and thymidine kinase for 5-fluoro-2'-deoxyuridine and 5-trifluorothymidine.

TABLE 3. Anti-influenza virus activity of T-705 and related carboxamide analogues in WT- and HGPRT-deficient MDCK cells

Compound	Antiviral activity (μM) determined by RT-qPCR[b]			
	MDCK-WT cells		**MDCK-TG^{res} cells[a]**	
	EC_{90}	EC_{99}	EC_{90}	EC_{99}
T-705	6.2 ± 0.6	12 ± 0.5	>500	>500
T-1105	0.98 ± 0.32	2.5 ± 0.1	>500	>500
2-Pyrazinamide	>500	>500	>500	>500
6-Cl-3,5-diamino-2-pyrazinamide	>500	>500	>500	>500
Ribavirin base	>500	>500	>500	>500
Ribavirin	1.9 ± 0.2	3.6 ± 0.2	0.51 ± 0.07	1.4 ± 0.7

[a]MDCK-TG^{res} cells selected for resistance against 6-thioguanine, and shown to be HGPRT-deficient by phenotypic and genotypic characterization (see Fig. 3). MDCK-WT: MDCK-wild type cells.

[b]Antiviral activity determined by RT-qPCR based virus yield assay with influenza virus strain A/X-31, and expressed as EC_{90} or EC_{99}, i.e. compound concentration causing a 1-$\log_{10}$ or 2-$\log_{10}$ reduction in virus titer, respectively.

Data are the mean ± S.E.M. of two independent tests.

TABLE 4.
Effect of siRNA-mediated gene silencing on the inhibitory effect of the carboxamide analogues towards influenza virus vRNP activity.

Compound	EC_{50} (μM) for inhibition of influenza vRNP activity[a] after siRNA-mediated gene knockdown[b] for						IC_{50} (μM) for inhibition of polII[c]
	HGPRT	APRT	NAMPT	ADK	NC	CC	
T-705	88 ± 17**	8.0 ± 0.5	7.8 ± 1.9	12 ± 3	14 ± 4	11 ± 1	>500
T-1105	237 ± 35**	31 ± 9	40 ± 10	46 ± 7	40 ± 7	38 ± 4	>500
Ribavirin	5.5 ± 0.5	5.5 ± 0.0	5.0 ± 0.4	31 ± 10	4.7 ± 1.3	5.2 ± 1.0	>500
Nucleozin	1.6 ± 0.3	1.8 ± 0.2	2.0 ± 0.3	1.8 ± 0.3	1.9 ± 0.4	1.8 ± 0.1	43

[a]EC_{50}: 50% effective concentration producing 50% inhibition of influenza vRNP activity, estimated from the Firefly reporter signal.
[b]HEK293T cells were siRNA-transfected to silence the indicated genes (NC: negative control siRNA; CC: non-siRNA-transfected control cells). After 48 h, cells were transfected with the influenza vRNP-reconstituting plasmids and the firefly and Renilla reporter plasmids, and incubated with the test compounds. The luciferase activity was determined 24 h later.
[c]IC_{50}: compound concentration causing 50% reduction of the polII-dependent Renilla luciferase signal.
**$P<0.01$ *versus* the EC_{50} value obtained in the non-siRNA-transfected control cells (CC) (two-tailed Student's t-test).
Data are the mean ± S.E.M. of 3-5 independent tests.

Molecular Pharmacology Fast Forward. Published on August 1, 2013 as DOI: 10.1124/mol.113.087247
This article has not been copyedited and formatted. The final version may differ from this version.

TABLE 5.

Data collection and refinement statistics for human HGPRT in complex with T-705-RMP.

Crystal parameters	
Unit cell length *a, b, c* (Å)	46.89 x 73.40 x 109.13
Unit cell angle α, β, γ (°)	90 x 90 x 90
Space group	*I* 2 2 2
Crystal dimensions (mm)	0.08x0.02x0.01
Diffraction data[a]	
Resolution range (Å)	43.06-2.73 (2.89-2.73)
Observations	37,338 (4584)
Unique reflections	5283 (680)
Completeness (%)	100.0
[b]R_{merge}	0.143 (0.651)
[c]$R_{p.i.m.}$	0.070 (0.272)
$/<\sigma(I)>$	*13.16 (3.0)*
Subunits per asym.unit	*1*
Refinement	
R_{work}	*24.99*
R_{free}	*27.02*
RMSD bond lengths (Å)	*0.007*
RMSD angles (°)	*0.7*
[d]*Clashscore*	
Components of the asymmetric unit	
Protein	*4-102, 123-217*
Inhibitors	*1*
Water	*40*
Ramachandran plot (%)	
Favoured	*94.6*
Outliers	*2.7*

[a]*Values in parentheses are for the outer resolution shell.*

[b] $R_{merge} = \sum_{hkl}\sum_i \left|I_i(hkl) - \left(I(hkl)\right)\right| / \sum_{hkl}\sum_i I_i(hkl)$

[c] $R_{p.i.m.} = \sum_{hkl}\left[\frac{1}{[N(hkl)-1]}\right]^{1/2} \sum_i \left|I_i(hkl) - \left(I(hkl)\right)\right| / \sum_{hkl}\sum_i I_i(hkl)$

where $I_i(hkl)$ is the observed intensity and is the average intensity obtained from multiple observations of symmetry related reflections. [d]*Clashscore is defined as the number of bad overlaps ≥ 0.4 Å per thousand atoms.*

Figure 1

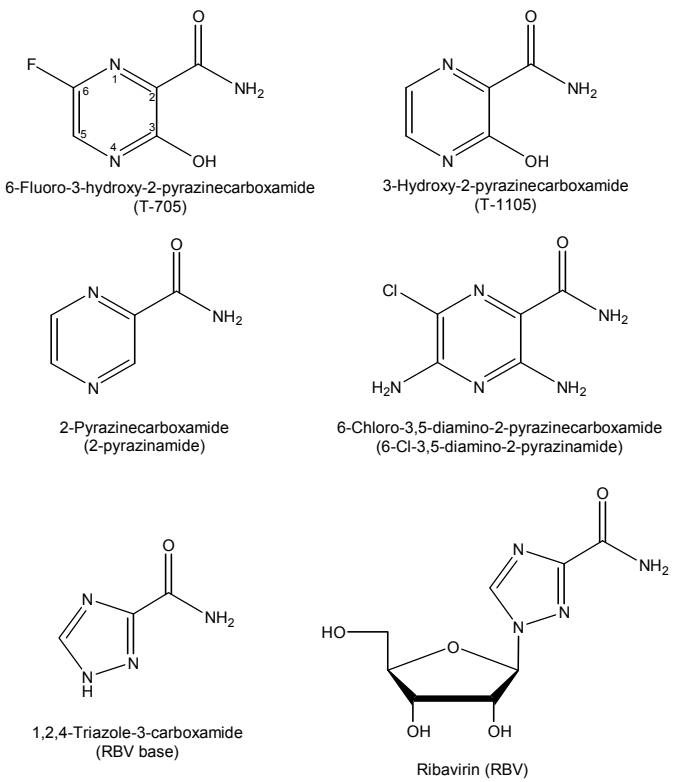

Figure 2

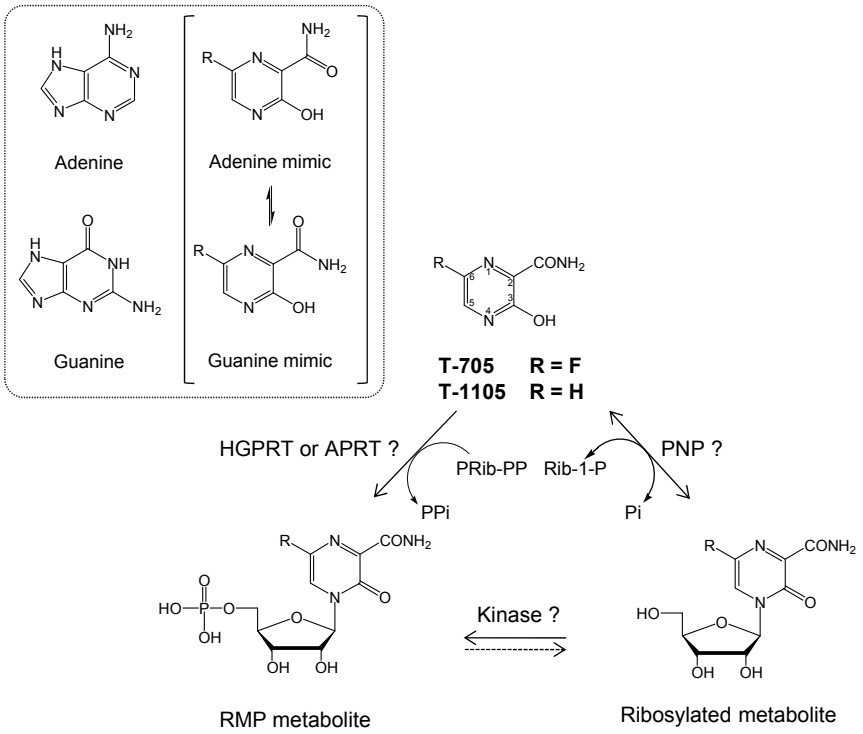

Figure 3

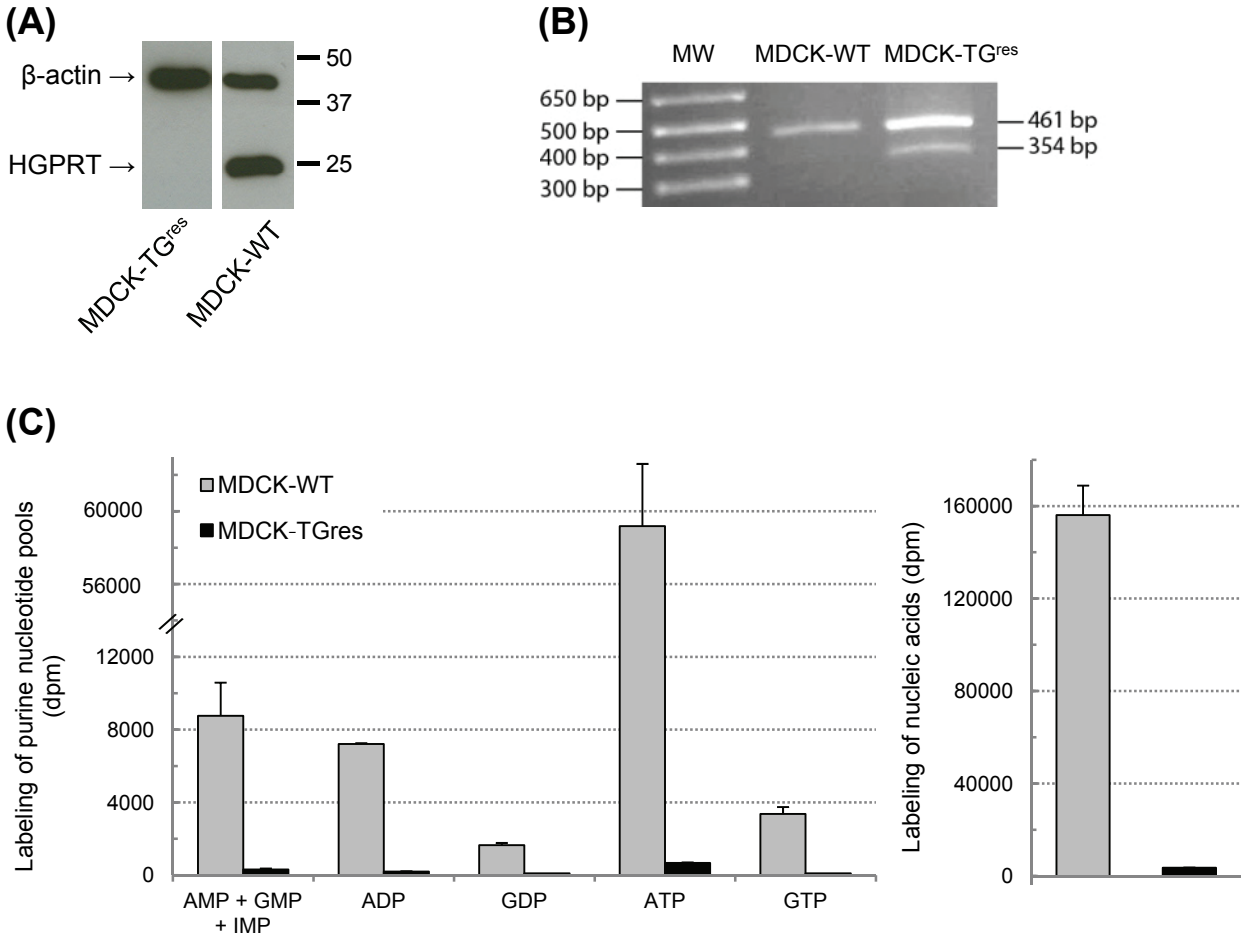

Figure 4

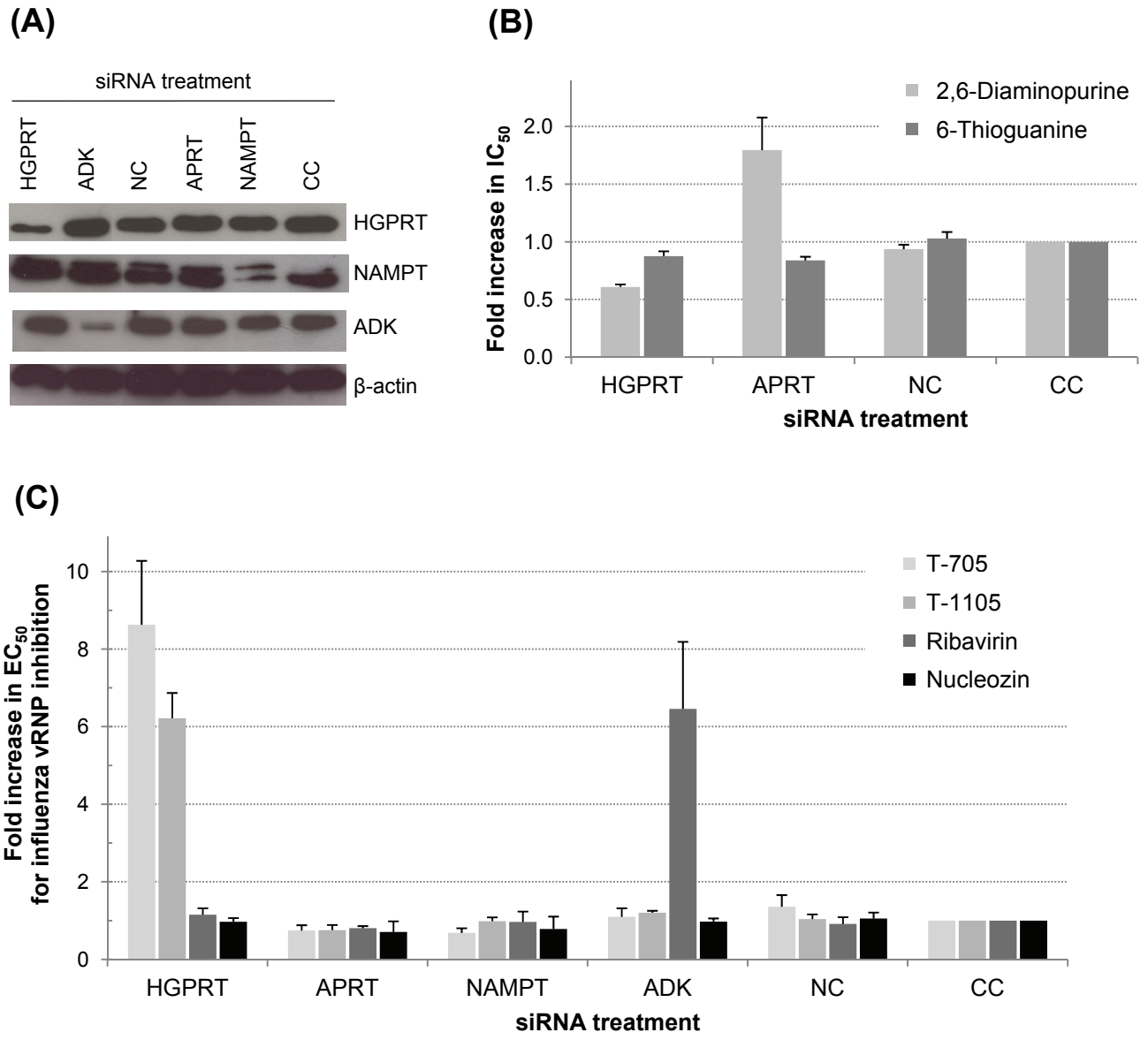

Figure 5

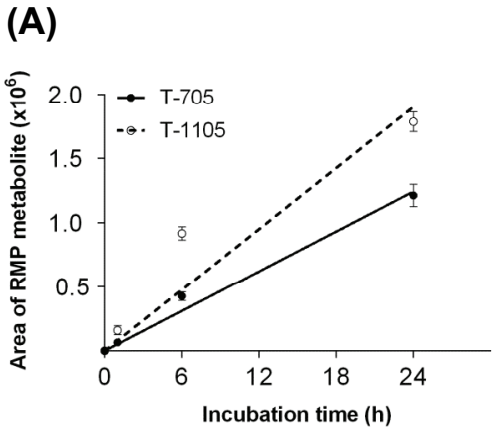

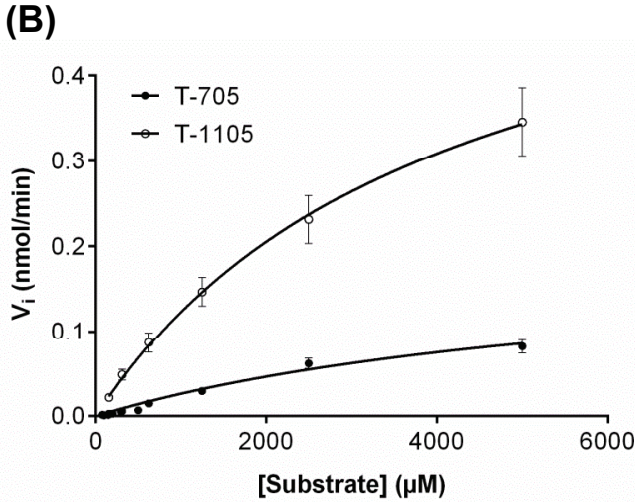

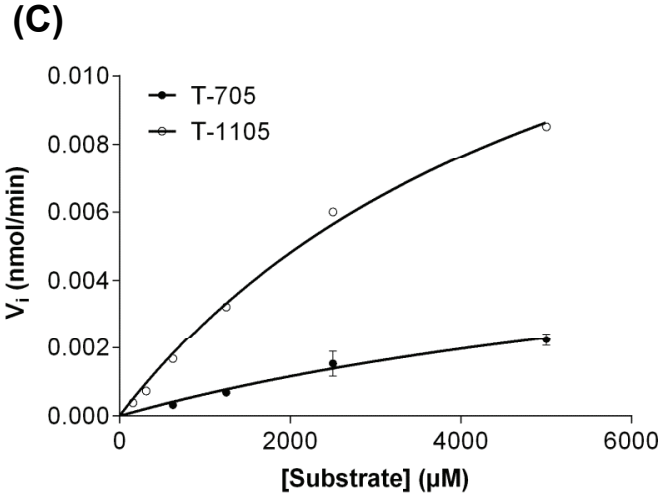

	K_m^{app} (μM)	k_{cat}/K_m^{app} ($s^{-1}.\mu M^{-1}$)
T-705	6426	0.000027
T-1105	4069	0.00014
Hypoxanthine	3.6	0.13
Guanine	5.4	0.14

Figure 6